Computers and Chemical Engineering 169 (2023) 108080

Contents lists available at ScienceDirect

Computers and Chemical Engineering

journal homepage: www.elsevier.com/locate/compchemeng

Sorption enhanced steam methane reforming in a bubbling fluidized bed reactor: Simulation and analysis by the CPFD method

Antonio Di Nardo [a,*], Giorgio Calchetti [a], Andrea Di Carlo [b], Stefano Stendardo [a]

[a] ENEA, Energy Technology Department, Casaccia Research Center, Via Anguillarese 301, Rome 00123, Italy
[b] Università dell'Aquila, Piazzale E. Pontieri 1, L'Aquila 67100, Italy

ARTICLE INFO

Keywords:
Sorption enhanced steam methane reforming
Calcium looping
Bubbling fluidized beds
Computational particles fluid dynamics

ABSTRACT

This work reports the modelling and simulation results of a bubbling fluidized bed reactor using the Computational Particle Fluid Dynamics (CPFD) method of the Barracuda® software. The reactor under investigation is the carbonator installed in the ENEA ZECOMIX research infrastructure, where Steam Methane Reforming (SMR) happens simultaneous with CO_2 capture via solid sorbents. In this intensified process, namely Sorption Enhanced Steam Methane Reforming (SE-SMR), steam methane reforming is coupled with high temperature CO_2 sorption and calcium looping (CaL) process, in order to increase the H_2 yield, beyond thermodynamic limits. Currently, the reactor is operated in batch mode and is used also for sorbent regeneration, by switching the fluidizing gas flow from steam/methane to oxy-burner combustion products. With the aim of studying the process when it is operated as a closed loop, in this paper the reactor is continuously fed by a fresh sorbent flow and a riser/calciner reactor for sorbent regeneration, to be connected with the carbonator, has been sized. The continuous circulation of solid material between the two reactors ensures the maintenance of different operating temperatures and therefore greater operational optimization.

The numerical analysis presented in this paper will serve as a valid support for the experimental activities. For this purpose, a sensitivity study on the SE-SMR process has been conducted, by varying the main operating conditions (e.g. sorbent conversion, sorbent/catalyst ratio, fluidizing gas flow), to evaluate the hydrogen purity yield. Two different kinetic mechanisms have been compared for the gas phase reactions. A post-processing routine has been written, in order to analyze bubbles sizes and velocities inside the fluidized environment. The effect of sorbent and catalyst particles segregation has been also investigated. The same modelling approach has been used for the sizing of the fast riser calciner reactor.

1. Introduction

Today the vast majority of all produced hydrogen is derived from fossil fuels (natural gas and coal) and it is responsible for approximately 830 Mt of CO_2 emitted each year (IEA, 2019). Steam methane reforming (SMR) is one of the most widespread industrial processes for hydrogen production. In order to produce such a large amount of H_2 and meet the future massive requests, the research community has focused its efforts on CO_2 capture systems implementation in current H_2 production processes, which can play a key role in the perspective of a net zero emissions economy by 2070.

Alternative approaches have been proposed, but the most promising method for large scale H_2 production is Sorption-Enhanced Steam Methane Reforming (SE-SMR). This process is able to increase the hydrogen yield and lower the operating temperatures (650°C). It is currently under investigation in the ENEA Research Infrastructure of the European Carbon Dioxide Capture Storage Laboratories (ECCSEL), named ZECOMIX (Zero Emission of Carbon with MIXed technologies), at semi-industrial scale. This intensified process couples SMR with high temperature CO_2 capture, via calcium looping (CaL) process. SE-SMR uses high temperature solid sorbents, for simultaneous separation of CO_2 and conversion of other carbon containing gases (CO and CH_4) into both H_2 and CO_2. It provides a step-change in efficiency, because it

Abbreviations: CPFD, Computational Particle Fluid Dynamics; SMR, Steam Methane Reforming; SE-SMR, Sorption Enhanced Steam Methane Reforming; CaL, Calcium looping; ECCSEL, European Carbon Dioxide Capture Storage Laboratories; ZECOMIX, Zero Emission of Carbon with MIXed technologies; TFM, Two-Fluid Model; MP-PIC, Multi-Phase Particle-In-Cell; DEM, Discrete Element Method; EMMS, Energy Minimization Multi-Scale; CFB, Circulating Fluidized Bed; XF, Xu and Froment; NK, Numaguchi and Kikuchi; LES, Large Eddy Simulation.

* Corresponding author.
E-mail address: antonio.dinardo@enea.it (A.D. Nardo).

https://doi.org/10.1016/j.compchemeng.2022.108080
Received 19 October 2021; Received in revised form 23 May 2022; Accepted 24 November 2022
Available online 26 November 2022

Nomenclature

a,b	Product layer diffusivity constants
$\boldsymbol{A_p}$, A_p	Particle acceleration, Particle surface
C	Smagorinsky coefficient
C_{CO2},$C_{CO2,eq}$	CO_2 and CO_2 equilibrium concentration
C_d	Drag coefficient
$C_{p,i}$	Constant press. specific heat for species i
C_V	Constant volume specific heat
D	Turbulent mass diffusion rate
D_p	Drag function
D_{pl},$D_{pl,0}$	Product layer diffusivity and diffusivity coefficient
E_{WGS},E_{SMR}	Activation energies NK model
E	Calcination Arrhenius reac. rate activation energy
$\boldsymbol{F}$	Fluid-particles momentum transfer
$f^{\circ}{}_{CaO}$	CaO volume fraction in fully calcinated conditions
f_D	Particle distribution func. for part. vel.
f_p	Particle distribution function
$\boldsymbol{g}$	Gravity acceleration
h_g	Gas henthalpy
h_p	Particle hentalpy
$k_{1,2,3}$	Arrhenius Reaction rates XF model
$k^0{}_{SMR}$,$k^0{}_{WGS}$	Pre-exponential factors Arrhenius reac. rate NK model
k_0	Calcination Arrhenius reac. rate pre-exponential factor
k_c	Calcination Arrhenius reac. rate
k_{cbn}	Carbonation reaction rate constant
K_{eqi},$K_{eq,SMR}$,$K_{eq,WGS}$	Equilibrium constant of reaction XF and NK models
K_i	Adsorbition constant of species i XF model
M	Mixing index
m_p	Particle mass
$N^{\circ}{}_{CaO}$	Number of CaO moles per unit volume in fully calcinated conditions
$Nu_{g,p}$	Nusselt number
p	Gas pressure
$P_{CO2,eq}$	CO_2 equilibrium partial pressure
P_i	Partial pressure of species i
P_p	Particle collision normal stress constant
$\boldsymbol{q}$	Gas heat flux
$\dot{q}_D$	Enthalpy diffusion term
$\dot{Q}$	Energy source per unit volume
R	Universal gas constant
Re	Reynolds number
r_i,r_{SMR},r_{WGS}	Reaction rate XF and NK models
r_p	Particle radius
r_s	Rate of change of CaO conversion
S_h	Gas solid energy exchange
T_g,T_p,T	Gas temp., Particle temp., Temperature
u_i,$\boldsymbol{u_g}$	Gas velocity
$\boldsymbol{u_p}$	Particle velocity
$\bar{\mathbf{u}}_{\mathbf{p}}$	Local mass avereged particle velocity
X	Particle conversion
X_{CaO}	CaO conversion
$\boldsymbol{x_p}$	Particle position
$Y_{g,i}$	Species mass fraction
var	variance

Greek

α^{th}	Particle volume fraction threshold
β	Particle collision normal stress constant
$\delta^{\circ}{}_{CaO}$	Initial CaO grain diameter
$\delta\dot{m}_{i,chem}$	Net production rate of species
$\delta\dot{m}_p$	Gas mass prod. rate per volume
δ_{ij}	Dirac delta function
ϵ	Particle collision normal stress constant
ε_{cp}	Particle volume fraction close pack
ε_g	Gas volume fraction
ε_p	Particle volume fraction
λ_g	Thermal conductivity
μ_g	Gas viscosity
μ_t	Sub grid turbulent viscosity
ρ_g	Gas density
ρ_p	Particle density
$\sigma^{\circ}{}_{CaO}$	CaO grain surface area per unit particle volume, in fully calcined conditions
ς	ratio between molar volume of $CaCO_3$ and CaO
τ_D	Particle collision damping time
τ_g	Stress tensor
τ_p	Contact normal stress
Φ	Viscous dissipation

separates CO_2 at elevated temperatures (>600°C), providing for more efficient heat integration options, not available in technologies where separation occurs at lower temperatures. It matches both endothermic and exothermic heat requirements of associated reactions and sorbent regeneration, in an integrated in situ approach.

The numerical simulation of the SE-SMR process has been carried-out using different approaches in the literature. Many of them are based on simplified, pseudo-homogenous or heterogeneous, one-dimensional or two-dimensional models and deal with fixed-bed reactors (Faheem et al., 2021; Shahid et al., 2021; Diglio et al., 2018; Abbas et al., 2019; Ping and Wu, 2019; Huang et al., 2021). These simplified models are able to give useful information on the phenomenon for fixed-bed reactors but a complete insight can be obtained only by resorting to CFD simulation in case of fluidized beds. In fluidization, CFD can simulate fluid-solid interactions accurately and predict the macroscopic phenomena involved in particulate systems. CFD plays an important role in engineering nowadays and it is commonly used to complement experimental studies. CFD-based simulations have some advantages compared to experimental measurements, as for example the reduced design time, the analysis or preliminary assessments of systems in difficult conditions to reply and the evaluation of hard to measure system quantities. The availability of ever more powerful computers now makes CFD simulation widely accessible. The SE-SMR process was studied by Lindborg and Jakobsen (2009) using an in-house TFM code in a two-dimensional cylindrical bubbling fluidized bed. Lithium zirconate was used as CO_2 sorbent, $NiO/MgAl_2O_4$ as catalyst and it was verified as wide reactors are favourable in industrial applications for obtaining high mass throughputs. The authors reported how at elevated pressures and/or higher fluidization velocities an increased bed heights is required and how internal circulation and spatial temperature variations affect the reactor performance. Compared to the traditional SMR process, a significant increase in hydrogen concentration was calculated, under the same operating conditions. Wang et al. (2014) carried out the simulation of a circulating fluidized bed (CFB) reactor, using an extended 3D version of the TFM code used in Lindborg and Jakobsen (2009). SE-SMR was conducted in a downer in bubbling fluidization regime, while CaO sorbent regeneration was conducted in a riser in fast fluidization regime. The two reactors were linked by a fixed solid flux. In comparison to the same process conducted in a batch bubbling fluidized bed reactor, while SMR is near equilibrium in both cases, in the CFB the CO_2 concentration in the sorbent material is lower. For that reason, the authors concluded that a large sorption capacity is unnecessary if the process is operated in continuous mode with respect to the batch mode. The SE-SMR process performance of a bubbling fluidized bed reactor was studied by Chao

et al. (2017), using an in-house 2D Eulerian-Eulerian TFM code. A lab-scale and an industrial-scale SE-SMR fluidized bed reactors were simulated and the performance of the process was compared with the conventional SMR process. The reforming catalyst employed in this study was a standard NiO/Al_2O_3 and $CaO/Ca_{12}Al_{14}O_{33}$ was selected as sorbent, on the basis of earlier studies. The authors analysed the influences of the superficial gas velocities and the solid loading on the reactor performance. Chen et al. (2013b) carried out two-dimensional CFD simulations of the SE-SMR process in a cylindrical bubbling fluidized bed reactor at relatively low temperature, using ANSYS-FLUENT® and an Eulerian-Eulerian TFM approach. The influence of the main operating conditions was examined and two sorbent materials were compared, hydrotalcite and lithium-zirconate. A dry H_2 concentration of 87% was obtained for hydrotalcite at 500°C, 0.1 MPa and for a superficial velocity of 0.15 m/s, higher than that obtained for lithium-zirconate. If methane conversion was increased at low pressure, CO_2 capture was improved at high pressure. In addition, it was observed how sorbents with faster kinetics can also enhance the steam methane reforming. Di Carlo et al. (2017) simulated the SE-SMR process in a bubbling fluidized bed of bifunctional combined sorbent-catalyst materials, by two-dimensional TFM simulations in ANSYS-FLUENT®. The positive effect of carbon dioxide capture on the reforming process was shown and it was provided an estimate for the heat flux that is required to operate the reactor in stationary temperature conditions. In particular, they reported that the required thermal input is reduced by the exothermic sorption process and can be supplied by the solid circulation between the SE-SMR reactor and the high temperature calciner.

It is evident how the process has been usually studied in batch, by means of two-dimensional Eulerian-Eulerian TFM simulations. Moreover, sorbent regeneration is generally not addressed, except in Wang et al. (2014), where however the authors adopted the TFM for the riser simulation, which can be inaccurate in highly diluted solid flows. In this paper a different numerical approach has been used, i.e. the Eulerian-Lagrangian CPFD method (Snider and Banerjee, 2010; Snider et al., 2011; O'Rourke et al., 2009) of the Barracuda® software. The choice of the CPFD method was dictated by its numerous advantages, which will be illustrated in details the next section. Several works that investigate the fluid dynamics of complex fluidized bed systems have been produced, using the CPFD method of the Barracuda® software. A three dimensional model of a circulating fluidized bed was validated by Thapa et al. (2016), using lab-scale experimental data and finding a good agreement regarding pressure drop and solid circulation rate, at various air feed rates. The model was also used to optimize the air feed positions that maximize the solid circulation rate. Liu et al. (2015) simulated a full-loop biomass gasifier, including chemical kinetics. The predicted gas composition and reactor temperature profiles matched the experimental measurements quite well. Clark et al. (2013) carried out simulations of a cold circulating fluidized bed for carbon capture process and concluded that the model was able to satisfactorily predict the experimental pressure measurements.

Many studies concerning bubbling and entrained fluidized beds simulation that use Barracuda® can be found in the literature. A pseudo-2D bubbling fluidized bed of Geldart B particles was simulated by Liang et al. (2014), comparing the TFM model and Barracuda® results with the available experimental data. The authors found that the latter method reproduced particles velocities quite well, but resulted less accurate with regards to bubbles formation and coalescence. Karimipour and Pugsley (2012) studied a bubbling fluidized bed of Geldart A particles, focusing on bubbles properties and verified a good predictive capability of the model, without the need to modify the drag model, in contrast to similar studies conducted by the same group and based on the TFM approach. Feng et al. (2018) performed a parametric study of bubbling fluidized beds, using the MP-PIC technique, on which the CPFD method is based on, by substituting the homogeneous drag model with the Energy Minimization Multi-Scale (EMMS) drag model (Li and Kwauk, 1994). The adoption of the EMMS model increased the accuracy level of the results if compared to the experimental data (e.g. solid distribution and bed height).

This work addresses both the kinetic and fluid dynamics aspects of the SE-SMR process, using Barracuda® with the embedded EMMS drag model. The goal of the work is to study the SE-SMR process when the reactor is continuously fed instead of being operated in batch mode. For this purpose a riser/calciner to be connected to the currently existing carbonator has been sized for sorbent regeneration, in order to make continuous the entire CO_2 capture loop process. The experimental data of Di Carlo et al. (2010) have been used for model validation regarding the SE-SMR output gas composition. A post-processing routine has been written, in order to analyze bubbles dimensions and velocities inside the bubbling fluidized bed environment. Two kinetic mechanisms have been compared for the gas phase reactions and a sensitivity study has been conducted, by varying the main operating conditions (e.g. sorbent conversion, sorbent/catalyst ratio, fluidizing gas flow) and evaluating the hydrogen purity yield. The numerical results obtained in this paper will allow to efficiently guide the experimental activities, with a considerable saving of time and technical and economic resources.

2. Fluidized beds CFD numerical models comparison

Fluidized beds CFD simulation can be approached mainly with three different methods: Two-Fluids Model (TFM) (Gidaspow, 1994; Gidaspow et al., 2004), Discrete Element Method (DEM) (Deen et al., 2007; Zhu et al., 2007) and Multi-Phase Particle-In-Cell method (MP-PIC) (Snider, 2001). While the first belongs to the Eulerian-Eulerian models class, the others pertain to the Eulerian-Lagrangian methods. The Eulerian-Eulerian TFM is the most used in the research community for the SE-SMR process CFD simulation and has been widely used for fluidized beds in general. In the TFM phases are treated as a pseudo continuum. It averages fluids and solids equations by a statistical procedure and this averaging procedure leads to many unclosed terms. The accuracy of the Eulerian-Eulerian approach heavily relies on the empirical constitutive equations needed for the unclosed terms modeling, as for example viscous stresses and particle-particle stresses. The equations set has to be solved for each dimension and particle type and size variation that occurs for example in reacting flows cannot easily accounted for. This leads to a very large set of equations that are not suitable to be solved with CPU-GPU hybrid computing. Furthermore, while the continuous description of the solid phase can be justified in some flow regimes, it becomes inaccurate in highly diluted solid flows and the assumption of high collision frequencies is questionable (Baker et al., 2020; Zhang et al., 2021). In addition, the model could result in an overestimated solid mixing in fluidized beds and presents also limitations in describing the gas-particle, particle-particle and particle-wall interactions.

In the Eulerian-Lagrangian approach, the gas phase is treated as a continuum while the dispersed solid phase is calculated by solving the particles equation of motion, given by the Newton's second law, accounting for solid and fluid turbulence, heat, mass and momentum exchanges. The DEM methods are based on the calculations of a limited number of particles, supposed spherical of different diameters, interacting with each other by means of contact forces and with the fluid phase, through a drag model. Being the particles interrelated with each other, CPU–GPU hybrid computing results complicated. The CPFD method of the Barracuda® software used in this work, which is based on the MP-PIC method, adopts the Lagrangian-Eulerian approach, but instead of calculating the trajectories of each single particle, they are grouped by size, species, etc., in computational particles. Particles collisions are not directly calculated but modelled as spatial gradients calculated on the Eulerian grid, by an isotropic solid stress function, depending on solid volume fraction, and then interpolated back on the discrete particles. For an accurate interpolation, the size of the physical particles have to be small enough compared to the Eulerian grid. Gaseous and solid phases are fully coupled by species, momentum and

energy transfer. The immediate consequence is that industrial-scale reactors and systems with a large number of particles can be simulated at a relatively low computational cost. Particle size distribution and reaction kinetics are easily accounted in this model, since each particle is tracked individually. The method is suitable for different fluid-solid flow regimes, from bubbling regimes near to close pack limit as in the carbonator, to diluted regimes as in the calciner. Since particles move independently from each other, a larger time-step can be adopted and it is possible to take the advantage of graphic processors GPU for parallel calculation. The CPFD method allows long time simulations since works on coarse meshes, without loss of accuracy.

The choice of a proper drag model is crucial for a correct prediction of the operating parameters of a fluidized bed (e.g. gas and solid fluxes, residence time, etc.). Chen et al. (2013a) compared Barracuda® and TFM simulation results of a CFB riser. The CPFD method of Barracuda® with the Wen-Yu/Ergun drag model qualitatively captured the bottom-dense, upper-dilute and core-annulus heterogeneous structures, but they found that the momentum transfer was overestimated, while the TFM in conjunction with the EMMS drag model gave more accurate results. In this regard Li et al. (2012) introduced the EMMS model in a MP-PIC code to simulate the gas-solid flow in a CFB riser. Calculation results showed higher accuracy in predicting the macroscopic bottom dense and top dilute axial solid distribution, the core-annular radial distribution, the meso-scale local particle aggregation, as well as the solid flux, compared to homogenous drag models. Tu and Wang (2018) compared the EMMS and the Wen-Yu drag model, in the simulation of a complex full-loop tridimensional CFB riser using Barracuda®. The superior performances of the EMMS drag model were demonstrated in predicting the axial pressure distribution, especially in the dense region, and the axial S-shape and radial M-shape solid volume fraction profiles. Even if the model was introduced to properly simulate clusters in CFB risers, in the paper of Shi et al. (2011) an EMMS bubble-based modified version was presented, where the meso-scale structure was characterized with bubbles instead of the original EMMS model clusters. Therefore, the heterogeneous EMMS drag model has been adopted in this work, given its superior performance compared to homogeneous models.

2.1. CPFD methods governing equations

The conservation equations of momentum and others scalar variables are solved by the finite volumes method, using a staggered grid. The flow is compressible and given the operating conditions of pressure and temperature, the ideal gas equation of state is used for gas species partial pressure. The volume averaged gas mass, momentum, energy and species transport equations are:

Gas mass conservation equation

$$\frac{\partial(\varepsilon_g\rho_g)}{\partial t}+\nabla\cdot(\varepsilon_g\rho_g\boldsymbol{u}_\mathbf{g})=\delta\dot{m}_p \tag{1}$$

Gas momentum conservation equation

$$\frac{\partial(\varepsilon_g\rho_g\boldsymbol{u}_\mathbf{g})}{\partial t}+\nabla\cdot(\varepsilon_g\rho_g\boldsymbol{u}_\mathbf{g}\boldsymbol{u}_\mathbf{g})=-\nabla p+\boldsymbol{F}+\varepsilon_g\rho_g\boldsymbol{g}+\nabla\cdot\varepsilon_g\tau_g \tag{2}$$

where ε_g, ρ_g, $\boldsymbol{u_g}$ are gas volume fraction, density and velocity respectively, p is gas pressure, $\boldsymbol{F}$ is the interphase fluid-particles momentum transfer rate per unit volume, defined below and τ_g is the stress tensor:

Stress tensor

$$\tau_{g,i,j}=\mu_g\left(\frac{\partial u_i}{\partial x_j}+\frac{\partial u_j}{\partial x_i}\right)+\frac{2}{3}\mu_g\delta_{ij}\frac{\partial u_k}{\partial x_k} \tag{3}$$

here μ_g is the sum of laminar and turbulent viscosity, defined in the following.

Gas energy conservation equation

$$\frac{\partial(\varepsilon_g\rho_g h_g)}{\partial t}+\nabla\cdot(\varepsilon_g\rho_g h_g\boldsymbol{u}_\mathbf{g})=\varepsilon_g\left(\frac{\partial p}{\partial t}+\boldsymbol{u}_\mathbf{g}\cdot\nabla p\right)+\Phi-\nabla\cdot(\varepsilon_g\boldsymbol{q})+\dot{Q}+S_h+\dot{q}_D \tag{4}$$

where h_g is gas enthalpy, Φ is viscous dissipation, $\dot{Q}$ is the energy source per unit volume, the term S_h represents the energy exchange from the solid phase to the gas phase, $\dot{q}_D$ is the enthalpy diffusion term and $\boldsymbol{q}$ is gas heat flux by conduction.

Gas species transport equations

$$\frac{\partial(\varepsilon_g\rho_g Y_{g,i})}{\partial t}+\nabla(\varepsilon_g\rho_g Y_{g,i}\boldsymbol{u}_\mathbf{g})=\nabla\cdot(\rho_g D\varepsilon_g\nabla Y_{g,i})+\delta\dot{m}_{i,chem} \tag{5}$$

where $Y_{g,i}$ is the gas mass fraction of each species, D is the turbulent diffusivity and last term is the source term due to reactions.

Turbulence is treated using Large Eddy Simulation (LES) approach (Piomelli, 1999) and the eddy-viscosity Smagorinsky models (Smagorinsky, 1963). In LES, large eddies are directly calculated and the subgrid-scale turbulence is modeled by an eddy-viscosity:

Large Eddy Simulation unresolved sub grid turbulent viscosity

$$\mu_t=C\rho_g\Delta^2\sqrt{\left(\frac{\partial u_i}{\partial x_j}+\frac{\partial u_j}{\partial x_i}\right)^2} \tag{6}$$

From forces balance on a particle, particle equation of motion is derived:

Particles acceleration equation

$$\boldsymbol{A}_\mathbf{p}=\frac{d\boldsymbol{u}_\mathbf{p}}{dt}=D_p(\mathbf{u}_\mathbf{g}-\mathbf{u}_\mathbf{p})-\frac{1}{\rho_p}\nabla p+\mathbf{g}-\frac{1}{\varepsilon_p\rho_p}\nabla\tau_p+\frac{\overline{\mathbf{u}}_\mathbf{p}-\mathbf{u}_\mathbf{g}}{\tau_D} \tag{7}$$

where ε_p, ρ_p and τ_p are particles volume fraction, density and contact normal stress, respectively, and D_p depends on the drag model adopted:

EMMS drag model

$$D_p=\frac{9}{2}\frac{\mu_g}{\rho_p}\frac{f_e}{r_p^2} \tag{8}$$

$$f_e=\begin{cases}\dfrac{1}{180\varepsilon_g}\left(c_0\dfrac{\varepsilon_p}{\varepsilon_g}+c_1Re\right) & \varepsilon_g<0.74\\ (c_2+c_3Re^{n_0})\omega & \varepsilon_g\geq 0.74\ and\ Re<1000\\ c_4\dfrac{Re}{24}\omega & \varepsilon_g\geq 0.74\ and\ Re\geq 1000\end{cases} \tag{9}$$

$$\omega=\begin{cases}c_5+\dfrac{c_6}{4(\varepsilon_g+c_7)^2c_8} & 0.74\leq\varepsilon_g<0.82\\ c_9+\dfrac{c_{10}}{4(\varepsilon_g+c_{11})^2c_{12}} & 0.82<\varepsilon_g\leq 0.97\\ c_{13}+c_{14}\varepsilon_g & 0.97<\varepsilon_g\leq 1\end{cases} \tag{10}$$

$$Re=\frac{\rho_g|\boldsymbol{u}_\mathbf{g}-\boldsymbol{u}_\mathbf{p}|}{\mu_g}\ and\ r_p=\left(\frac{m_p}{\frac{4}{3}\pi\rho_p}\right)^{1/3} \tag{11}$$

where: c_0=150, c_1=1.75, c_2=1.0, c_3=0.15, c_4=0.44, c_5=−0.576, c_6=0.0214, c_7=−0.7463, c_8=0.0044, c_9=−0.0101, c_{10}=0.0038, c_{11}=−0.7789, c_{12}=0.0040, c_{13}=−31.8295, c_{14}=32.8295, n_0=0.687.

Particle position is then calculated as:

$$\frac{d\boldsymbol{x}_\mathbf{p}}{dt}=\boldsymbol{u}_\mathbf{p} \tag{12}$$

Particle-to-particle collisions are modeled by particle normal stress

τ_p. It is derived from particles volume fraction calculated from particle volume mapped to the grid and neglects particles size and velocity:

Particles collision normal stress

$$\tau_p = \frac{P_p \varepsilon_p^{\beta}}{\max\left[\left(\varepsilon_{cp} - \varepsilon_p\right), \varepsilon\left(1 - \varepsilon_p\right)\right]} \tag{13}$$

It is assumed that the particle temperature is uniform and the heat release, which depends only on surface reactions, is a source term for the gas phase. Fluid-to-wall (Yang, 2003) and fluid-to-particles (Fan and Zhu, 1998) heat exchange coefficients are calculated by empirical formulas. Particles energy equation is then:

Particles energy equation

$$C_V \frac{dT_p}{dt} = \frac{1}{m_p} \frac{\lambda_g N u_{g,p}}{2 r_p} A_p \left(T_g - T_p\right) \tag{14}$$

The dynamics of the solid phase is obtained by solving a transport equation for the particle distribution function (PDF) f_p:

Particles distribution function:

$$\frac{df_p}{dt} + \frac{\partial\left(f_p \boldsymbol{u}_\mathbf{p}\right)}{dx} + \frac{\partial\left(f_p \boldsymbol{A}_\mathbf{p}\right)}{du_p} = \frac{f_D - f_p}{\tau_D} \tag{15}$$

where f_d is the particle distribution function for the local mass averaged particle velocity. From f_p is possible to calculate particles volume fraction ε_p, momentum $\boldsymbol{F}$, mass $\delta\dot{m}_p$ and energy S_h transfer terms:

Particles volume fraction

$$\varepsilon_p = -\int\int\int f_p \frac{m_p}{\rho_p} dm_p d\boldsymbol{u}_\mathbf{p} dT_p \tag{16}$$

Momentum transfer between phases

$$\boldsymbol{F} = -\int\int\int f_p \left\{ m_p \left[D_p \left(\boldsymbol{u_g} - \boldsymbol{u_p}\right) - \frac{\Delta p}{\rho_p} \right] + \boldsymbol{u_p} \frac{dm_p}{dt} \right\} dm_p d\boldsymbol{u}_p dT_p \tag{17}$$

Mass transfer between phases

$$\delta\dot{m}_p = -\int\int\int f_p \frac{dm_p}{dt} dm_p d\boldsymbol{u}_p dT_p \tag{18}$$

Particles mass changes due to chemical reactions, according to the reaction rates reported in paragraphs 3.2-3.3.

Conservative energy exchange term

$$\begin{aligned} S_h = \int\int\int f_D \Bigg\{ & m_p \left[D_p \left(\boldsymbol{u_p} - \boldsymbol{u_g}\right)^2 - C_V \frac{dT_p}{dt} \right] \\ & - \frac{dm_p}{dt} \left[h_\mathbf{p} + \frac{1}{2} \left(\boldsymbol{u_p} - \boldsymbol{u_g}\right)^2 \right] \Bigg\} dm_p d\boldsymbol{u}_p dT_p \end{aligned} \tag{19}$$

Particle to wall interaction is accounted by momentum normal and tangential retention coefficients, that are defined as the fraction of the normal and tangential component of the particle momentum that is retained by the particle after collision with the wall and have been set equal to 0.5 and 0.85, respectively. A value of 0.5 indicates that 50% of the momentum (and 25% of the kinetic energy since kinetic energy varies with the square of velocity) is retained. Since in the real world particles are not perfectly round and walls are not perfectly smooth, a stochastic diffuse bounce model can be used. Only the direction of the particle reflection is affected by the diffuse-bounce model, but not the velocity magnitude.

3. Reaction models

3.1. Gas phase reactions kinetic mechanisms

The SMR process has been widely studied and several kinetic mechanisms are available, each of them pertaining certain operating conditions. The Xu and Froment (1989) kinetic mechanism has been extensively used in CFD simulations (Di Carlo et al., 2010; Wang et al., 2011; Chen et al., 2013b; Wang et al., 2014; Chao et al., 2017). A TFM in-house code with the XF kinetic mechanism was used by Wang et al. (2011) for the simulation of a SE-SMR bubbling fluidized bed reactor. It was found that CO_2 capture increases hydrogen production compared to a standard SMR process, that the time for breakthrough decreases by increasing gas superficial velocities and that the optimal value of steam-to-carbon ratio to achieve higher hydrogen production and lower steam consumption is about 4. Di Carlo et al. (2010) simulated a lab-scale SE-SMR fluidized bed, composed of dolomite and Ni-catalyst, by adopting a TFM approach combined with the XF kinetic mechanism and using effectiveness factors to account for pore diffusion resistance and particle surface phenomena. The implemented CO_2 capture model considered external mass fraction, intra-particle diffusion and chemical reactions. The model predicted a dry hydrogen mole fraction higher than 0.93 at 900 K, with a superficial gas velocity of 0.3 m/s and a sorbent/catalyst ratio higher than 2. Under these assumptions, the SE-SMR process turned out to be auto-thermic since the necessary heat for the reforming endothermic reactions could be entirely supplied by the exothermic carbonation reaction.

The physics of the SE-SMR process involves different phenomena to be considered, such as mass transfer resistance relative to the gas film around particles, pore diffusion and chemical reactions. As reported in Aloisi et al. (2017), in case of fluidized beds and small particles, the gradient of reactants concentration in the pores is very small for various bulk gas concentrations, as well as the gradient at the particle surface, so that a high effectiveness factor, over 90%, can be estimated. In the paper of Di Carlo et al. (2010), the authors calculated the effectiveness factors, that multiplies the intrinsic reaction rates, of the three reactions of the XF mechanism and that resulted equal to 0.7, 0.8 and 0.4.

The performance of two intrinsic mechanisms have been compared in this paper: the popular Xu and Froment (1989) and Numaguchi and Kikuchi (1988) chemical kinetic mechanisms. For the XF mechanism, experimental data were obtained using a Ni-MgO-Al_2O_3 catalyst, a hydrogen/methane feed equals to 1:25, temperatures in the range 500-575°C and pressures from 3 to 15 bar. Numaguchi and Kikuchi derived their data at higher catalyst temperatures (up to 887°C), and higher pressures (up to 25 bar). As observed by de Smet et al. (2001), the Ni-content in the second case was lower than the Ni-content in the first, but being the Ni-surface areas similar, the two models can be reasonably compared. It was shown how the reaction rate increases as pressure increases for the NK mechanism, while decreases for the XF mechanism because of the negative reaction order with respect to hydrogen concentration. However, in the simulations those differences are attenuated by the presence of large quantities of hydrogen.

Xu-Froment

$$\boldsymbol{CH_4 + H_2O \leftrightarrow 3H_2 + CO}$$

$$\boldsymbol{CO + H_2O \leftrightarrow H_2 + CO_2}$$

$$\boldsymbol{CH_4 + 2H_2O \leftrightarrow 4H_2 + CO_2}$$

$$r_1 = \frac{\frac{k_1}{P_{H_2}^{2.5}} \left[P_{CH_4} P_{H_2O} - \frac{P_{H_2}^3 P_{CO}}{K_{eq1}} \right]}{DEN^2} \tag{20}$$

$$r_2 = \frac{\frac{k_2}{P_{H_2}} \left[P_{CO} P_{H_2O} - \frac{P_{H_2} P_{CO_2}}{K_{eq2}} \right]}{DEN^2} \tag{21}$$

$$r_3 = \frac{\frac{k_3}{P_{H_2}^{3.5}} \left[P_{CH_4} P_{H_2O}^2 - \frac{P_{H_2}^4 P_{CO_2}}{K_{eq3}} \right]}{DEN^2} \tag{22}$$

$$DEN = 1 + K_{CO} P_{CO} + K_{H_2} P_{H_2} + K_{CH_4} P_{CH_4} + K_{H_2O} \frac{P_{H_2O}}{P_{H_2}} \tag{23}$$

Numaguchi-Kikuchi

$$\boldsymbol{CH_4 + H_2O \leftrightarrow 3H_2 + CO}$$

$$\boldsymbol{CO + H_2O \leftrightarrow H_2 + CO_2}$$

$$r_{SMR} = \frac{k^0_{SMR}\cdot e^{\left(-\frac{E_{SMR}}{RT}\right)}\cdot\left(P_{CH_4}\cdot P_{H_2O} - \frac{P_{CO}P^3_{H_2}}{K_{eq,SMR}}\right)}{P^{1.596}_{H_2O}} \tag{24}$$

$$r_{WGS} = \frac{k^0_{WGS}\cdot e^{-\frac{E_{WGS}}{RT}}\cdot\left(P_{CO}\cdot P_{H_2O} - \frac{P_{CO_2}P_{H_2}}{K_{eq,WGS}}\right)}{P_{H_2O}} \tag{25}$$

For the models equilibrium K_{eq}, adsorption K_i and reaction rate k_i constants, see the respective references.

3.2. CO_2 capture model

As far as the whole sorption mechanism of carbon dioxide $CaO+CO_2 \rightarrow CaCO_3$ is concerned, the model in Stendardo and Foscolo (2009) has been used. In this model a shrinking core approach is applied for the propagation of the reaction front inside the particle. With the CaO carbonation an outer layer of $CaCO_3$, becoming progressively more compact is developed and CO_2 encounters an increasing resistance through the product layer. A progressive reduction of porosity is also obtained as a consequence of the increase of grains volume and due to the different $CaCO_3$ and CaO molar volume ratio. The shrinking core approach is characterized by an exponentially decreasing diffusion coefficient (with CaO conversion) through the $CaCO_3$ layer and a first order surface reaction. The sorption rate expression, r_s, obeying the above requirements is:

$$r_s = \frac{N^0_{CaO}\cdot\sigma^0_{CaO}k_{CBN}(1-X_{CaO})^{2/3}\left(C_{CO_2} - C_{CO_2,eq}\right)}{1 + \frac{N^0_{CaO}k_{CBN}}{2D_{pl}}\delta^0_{CaO}\sqrt[3]{1-X_{CaO}}\left(1 - \sqrt[3]{\frac{1-X_{CaO}}{1-X_{CaO}+X_{CaO}\varsigma}}\right)} \tag{26}$$

where:

$$\sigma^0_{CaO} = 6\frac{f^0_{CaO}}{\delta^0_{CaO}} \tag{27}$$

where σ^0_{CaO} is the CaO grain surface area per unit particle volume, computed in fully calcined conditions and $\delta^0_{CaO}$is the initial CaO grain diameter.

$$D_{pl} = D_{pl,0}\exp\left(-aX^b_{CaO}\right) \tag{28}$$

is the product layer diffusivity coefficient; ς is the ratio between the molar volume of $CaCO_3$ and CaO, respectively; N^0_{CaO} is the number of CaO moles per unit volume of particle in fully calcined conditions and f^0_{CaO} its corresponding volumetric fraction. The rate of change of calcium oxide conversion, X_{CaO} is obtained as follows:

$$N^0_{CaO}\frac{\partial X_{CaO}}{\partial t} = r_s \tag{29}$$

The model constants, obtained from TGA sorption tests, are reported in Table 1.

Table 1
Carbonation constants used in the grain model.

N^0_{CaO}	21.9 kmol/m^3
σ^0_{CaO}	$2.22\cdot10^7$ m^2/m^3
k_{CBN}	$5.95\cdot10^{-7}$ m^4/(kmol s)
δ^0_{CaO}	$0.100\cdot10^{-6}$ m
ς	2.18
$D_{pl,0}$	$2\cdot10^{-5}$ m^2/s
a	22.5
b	0.03
f^0_{CaO}	0.37

3.3. Calcination reaction model

For the kinetic model of the calcination reaction $CaCO_3 \rightarrow CaO+CO_2$, through which the regeneration of the exhausted sorbent takes place, it can be supposed that the reaction occurs uniformly inside the particle. Based on what is reported in the literature (Fang et al., 2009; Martínez et al., 2012), a kinetic expression was used for $CaCO_3$ conversion, obtained using the grain model. In this model a porous structure of the particle is assumed, which consists of a grain matrix resulting from the various calcination cycles. For each grain the reaction takes place according to the shrinking core model, i.e. the reaction front propagates from the grain surface towards the interior. The average grain size greatly influences the amount of the active surface available for the reaction. It has been observed experimentally (Martínez et al., 2012) that under these conditions, the calcination reaction is controlled practically only by chemistry, since the resistance to mass diffusion inside the particles is negligible, for relatively small particles. Basically the calcination reaction depends on temperature and CO_2 partial pressure but it does not depend on $CaCO_3$ concentration. The kinetic equation which describes particle conversion X is:

$$\frac{dX}{dt} = k_c(1-X)^{\frac{2}{3}}\left(C_{CO_2,eq} - C_{CO_2}\right) \tag{30}$$

$$k_c = k_0\exp\left(-\frac{E}{RT}\right) \tag{31}$$

k_0=23794 m^3/(mol·s), E=150000 J/mol (Fang et al., 2009). The equilibrium CO_2 concentration is calculated from (Stanmore and Gilot, 2005):

$$P_{CO_2,eq} = 4.137e^7\exp\left(-\frac{20474}{T}\right) \tag{32}$$

4. ZECOMIX description

The SE-SMR reactor (Fig. 1 and 2) is a cylinder of diameter=1 m and height=4.5 m, insulated with 30 cm of two layers refractory enclosure. The feeding gas is supplied through a distributor plate realized as a series of perpendicular tubes that broke the gas jets, producing a quasi-homogenous velocity field and allowing to prevent particles clogging in the jets orifices.

The reactor was designed to produce, via steam methane reforming and water gas shift reactions, a flow rate of 5 kmol/h of H_2. In addition to hydrogen, however, carbon dioxide is also formed which, in the perspective of a zero-emission system, must be captured. The reactor is loaded with a Ni-based catalyst, to allow the steam methane reforming process to happen at lower temperatures and a Ca-based sorbent, which serves to decarbonize the flue gas and to enhance the steam methane reforming process. Calcium-based sorbents are available at low cost, but reduce their capture capacity over multiple capture/regeneration cycles. In this system calcined dolomite is used as sorbent (54.5% CaO, 45.5% MgO). A calcined sorbent/catalyst ratio of 2 in mass and a 4:1 steam/methane molar ratio flow of 500 m^3/h are the nominal operating conditions, since it is advisable to work with an excess of steam. The choice to work at atmospheric pressure was made to reduce the components and save on compression energy. The SE-SMR reactor, or simply carbonator, was designed to work at 650°C, because it represents a compromise between reactions thermodynamics, favored at lower temperatures and kinetics, which on the contrary is favored at higher temperatures. The reactor is operated in batch mode and the sorbent calcination and regeneration is conducted in the same reactor using oxy-burners hot products. A highly concentrated CO_2 gas for the final disposal is then obtained. After a cooling process the reactor returns to the initial condition and it is ready for another cycle.

In this simulation work instead, the reactor is continuously fed by a fresh sorbent flow and a riser/calciner reactor for sorbent regeneration

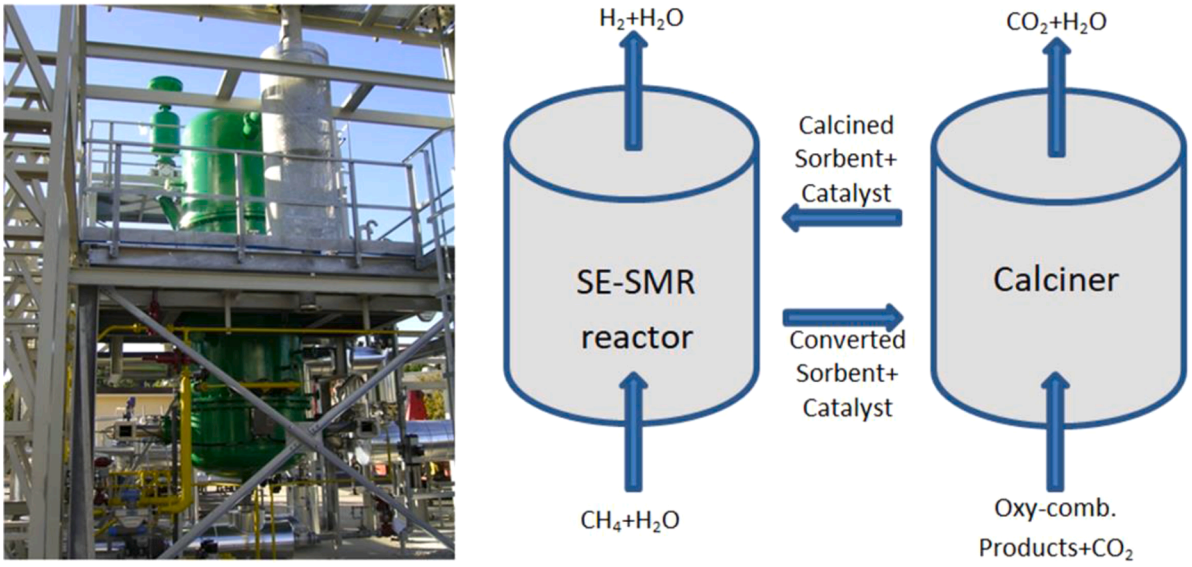

Fig. 1. SE-SMR batch reactor installed in the ECSSEL research infrastructure ZECOMIX (left). SE-SMR closed loop studied in this work (right).

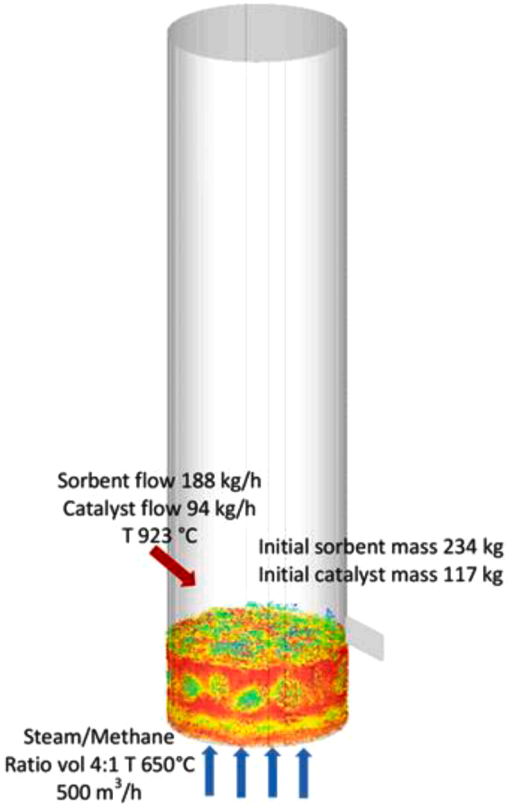

Fig. 2. SE-SMR reactor nominal operating conditions.

to be connected with the carbonator has been sized (Fig. 1). In this way there is a continuous circulation of solid material between the two reactors, that ensure the maintenance of the different operating temperatures and therefore greater operational optimization. The calciner has been sized with respect to diameter, height and gas flow rate, by fixing the inlet catalyst and sorbent flow rate to be regenerated and then recirculated in the carbonator (Table 2 and 4), coherent with a production of 5 kmol/h of H_2 and the consequent production of CO_2 that must be captured. One of the advantages of the SE-SMR process lies in the amount of heat necessary, which is considerably lower than a

Table 2
SE-SMR reactor nominal operating conditions.

Sorbent initial mass	234 kg
Catalyst initial mass	117 kg
Sorbent/Catalyst mass ratio	2
Sorbent and catalyst initial temp.	650°C
Calcined dolomite inlet mass flow	188 kg/h
Catalyst inlet mass flow	94 kg/h
Calc. dolomite and catalyst inlet temp.	923°C
Steam/Methane flow rate	500 m^3/h
Steam/Methane flow temperature	650°C
Steam/Methane molar ratio	4
Operating pressure	1 atm

conventional SMR process and it is supplied by the high temperature regenerated sorbent and catalyst, recirculating from the calciner. The loop-seal connections between the two reactors have not been studied here.

5. SE-SMR model validation

The presented numerical model has been validated as regards the output gas composition, using the experimental data reported in Di Carlo et al. (2010), involving a bubbling SE-SMR batch lab-scale reactor working in conditions similar to the ZECOMIX carbonator reactor. It is a cylinder of diameter 8 cm and the static bed height is 20 cm. The sorbent/catalyst ratio is 4 in volume and the fluidizing gas is composed of water vapor and methane, with a molar ratio of 4. The fluidization velocity was set to 0.15 m/s, three times the minimum fluidization velocity. Catalyst and calcined dolomite particle sizes range from 180 to 425 μm. The experiment was carried out at different operating temperatures. The XF model has been adopted for gas chemical reactions and the simulation time (1 min) is the one adopted by Di Carlo et al. (2010). In fact, since the sorbent capture capacity decreases with time, the product gas increases its carbon dioxide content. As shown in Fig. 3, where the hydrogen concentration is reported, a good agreement between simulation results and measurements has been obtained, with a maximum difference of 1%. The agreement between the experimental and the numerical results is comparable with that of other authors (Di Carlo et al., 2010; Chen et al., 2013b; Di Carlo et al., 2017). Often in these works, literature data relating to other systems, other than those under study, have been used to validate the model. An experimental-numerical comparison is however not always presented

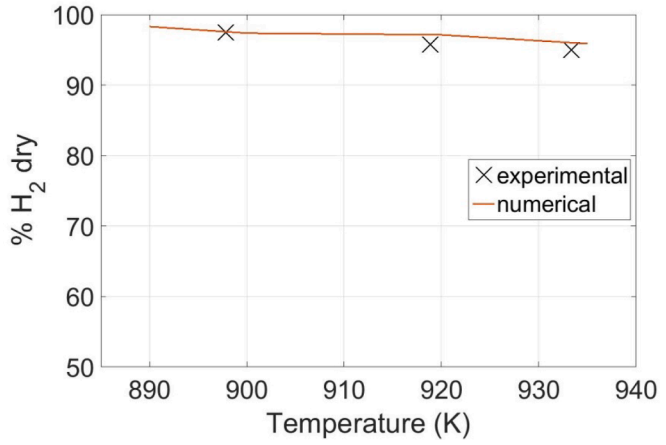

Fig. 3. Model validation. SE-SMR hydrogen concentration in the product gas for the lab-scale experimental reactor in Di Carlo et al. (2010).

(Wang et al., 2014; Chao et al., 2017). No differences in the product gas composition have been obtained using the effectiveness factors for the XF model calculated by Di Carlo et al. (2010) or by neglecting particle surface and pores diffusion resistances, as suggested by Aloisi et al. (2017). This second approach has been then followed for all the simulations in the subsequent paragraphs.

6. SE-SMR simulations results

6.1. Bubbles detection

The carbonator reactor is operated in the bubbling fluidization regime, for a nominal superficial velocity of 0.17 m/s. For the present analysis a sorbent particles composition corresponding to 60% converted calcined dolomite has been fixed (see the following discussion), for the reactor initial hold-up. The sorbent minimum fluidization velocity (ρ=1644 kg/m^3 at 60% conversion, diameter=500 μm) is about 0.09 m/s, at 650°C. The Ni-based catalyst (ρ=2200 kg/m^3) diameter has been set at 380 μm, in order to have a sorbent similar minimum fluidization velocity. Particles fluid dynamic behavior could be classified as belonging to Geldart B group. Reactor walls has been considered adiabatic. The scheme and the nominal operating conditions of the carbonator are reported in Fig. 2 and Table 2. The computational mesh is composed of about 80000 cubic cells (each element is 0.01269×0.01269×0.01269 m). Only the first meter in height of the reactor has been simulated in this case, since we are interested only in the bubbling phenomenon and in order to work on a finer mesh. The results grid independency has been verified. In particular, starting from a coarser mesh it has been progressively refined up to 80000 cells, when no further and significant changes have been observed in the results in terms of bubbles diameters and velocities distribution, resumed by the histograms in Fig. 7. In this regard it must be underlined that the CPFD method requires cells sizes such as they can contain a statistical significant number of particles to work properly. The present analysis has been conducted to study bubbles dimensions and evolution inside the bed. For this purpose a routine (flow-chart in Fig. 4) has been written to post-process the simulated particles volume fraction field. The first step consists in identifying and labeling each group of connected cells having particle volume fraction less than a fixed threshold α^{th} (red colored cells in the Fig. 5), that separates the bubbles from the rest of the domain. Two cells are 3D connected if they share a face, an edge or a corner. Each of those labeled regions of cells is then dilated adding a "peel" of cells all around, having then a volume fraction higher than the threshold (blue colored cells in the Fig. 5). It is now possible to extract the iso-surfaces, for the fixed volume fraction threshold, in form of a cloud of points coordinates that define bubbles boundaries (dashed line and triangles

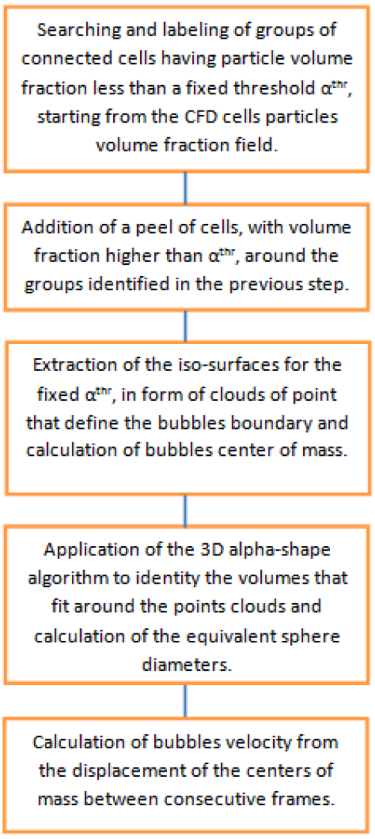

Fig. 4. Flow chart of the bubbles analysis routine.

vertices in Fig. 5) and calculate each center of mass. For each cluster of points the 3D alpha-shape algorithm (Edelsbrunner and Mücke, 1994; Julián et al., 2016) has been applied to calculate the void region volume and then the diameter of an equivalent volume spherical bubble.

Compared to convex methods, the concave 3D alpha-shape method allows for concave shapes and a tighten fit around the points. A drawback of this method is that it could restitute volume with holes, if the so-called alpha radius is too small. On the contrary, a value excessively high would give a loosen shape, close to convex hull. In the work of Julián et al. (2016) after the calculation of a single iso-surface related to a specified volume fraction threshold, the 3D alpha-shape method is applied to separate the single void zone obtained in individuals bubbles. In this way the number of bubbles detected is dependent upon the fixed alpha radius, which is related to mesh elements size. As specified by the authors, the method works better for a uniform concentration of mesh points and coalescence and break up phenomena could compromise an accurate bubbles discretization. In the present case instead, bubbles are detected using the procedure discussed above, before the application of the 3D alpha-shape algorithm, which is only used for bubbles equivalent diameter calculation. In the last step bubbles velocities are calculated from bubbles center of mass displacement between consecutive frames.

A parametric analysis has been conducted where the nominal value of the fluidizing gas mass flow rate has been increased by 1.5 and 2 times (Fig. 6). The calculation has been executed on a sufficient number of frames to make the results statistically significant and the bubbles with a diameter lower than the mesh size have been neglected in Figs. 7 and 8. For this reason in Fig. 8 the plots are cut for diameters lower than the mesh size and for heights lower than about 0.05 m. Small bubbles form in the deeper layers of the bed and start growing as they rise upward, due to gas entrainment and coalescence (Fig. 6). As the flow velocity increases, bubbles grow and transition from bubbling to slugging fluidization regime begins to appear (Fig. 6 from left to right). In fact small void regions are more and more difficult to be detected. Instead

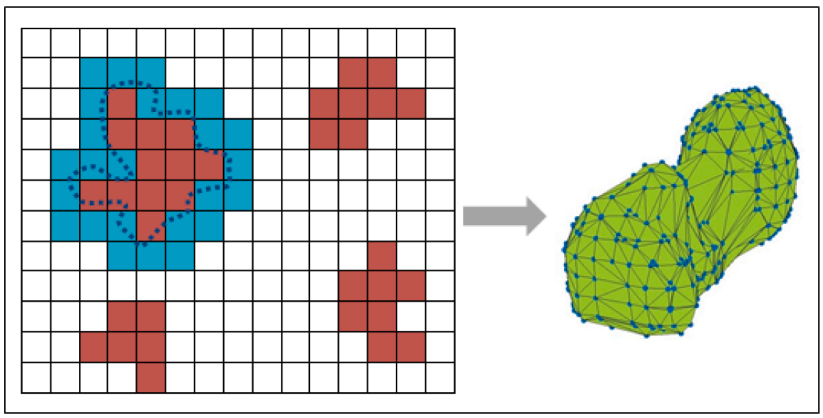

Fig. 5. Bubbles detection routine. Red squares: cells with particle volume fraction $< \alpha^{th}$. Blue dotted contour points: α^{th} iso-surface. Green triangulation: 3D alpha-shape volume.

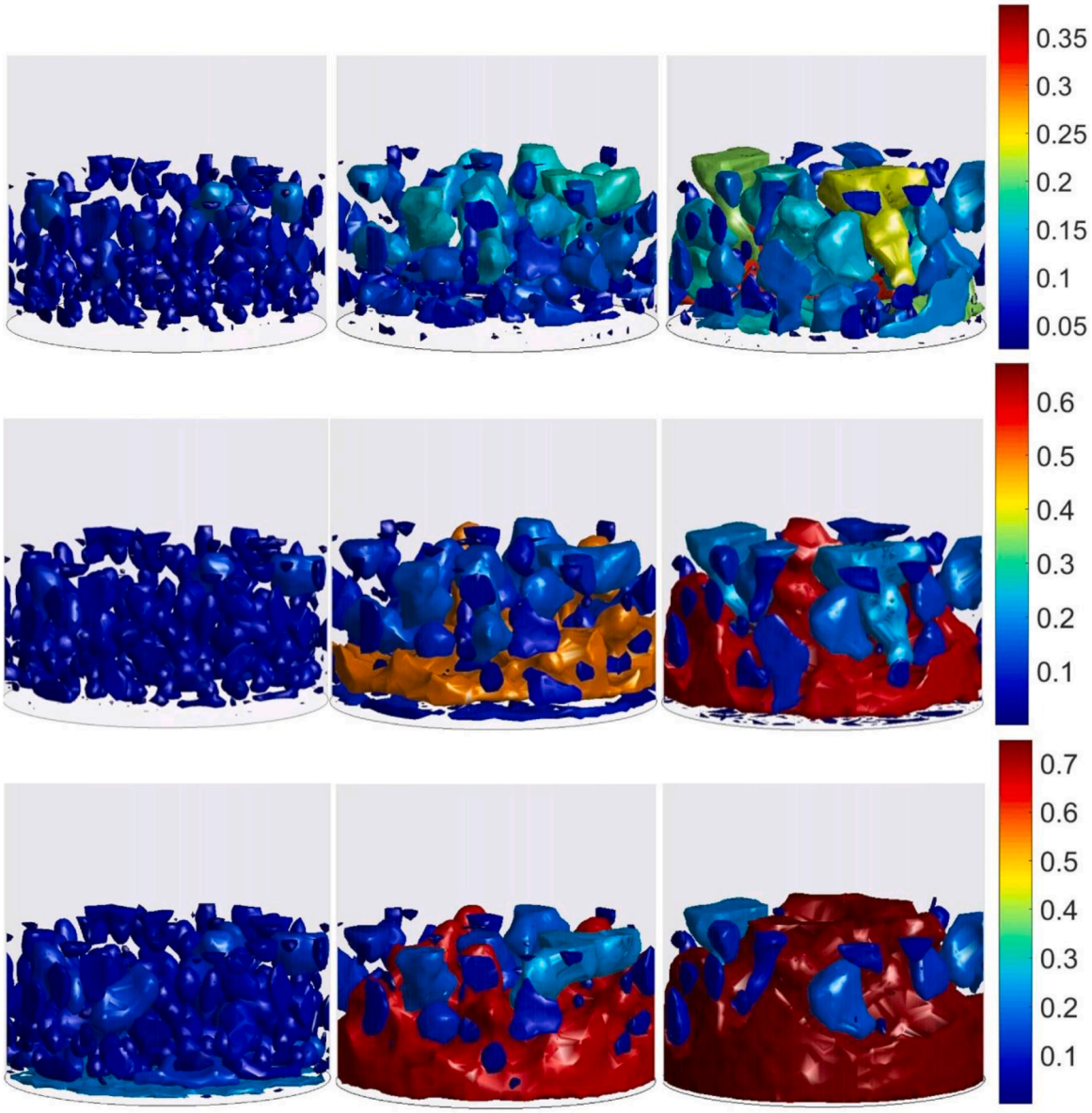

Fig. 6. SE-SMR reactor bubbles colored by bubbles diameter. Top α^{th} =0.2, middle α^{th} =0.3, bottom α^{th} =0.4. Left nominal flow rate=500 m^3/h of steam/methane, middle 1.5xnominal flow rate, right 2xnominal flow rate.

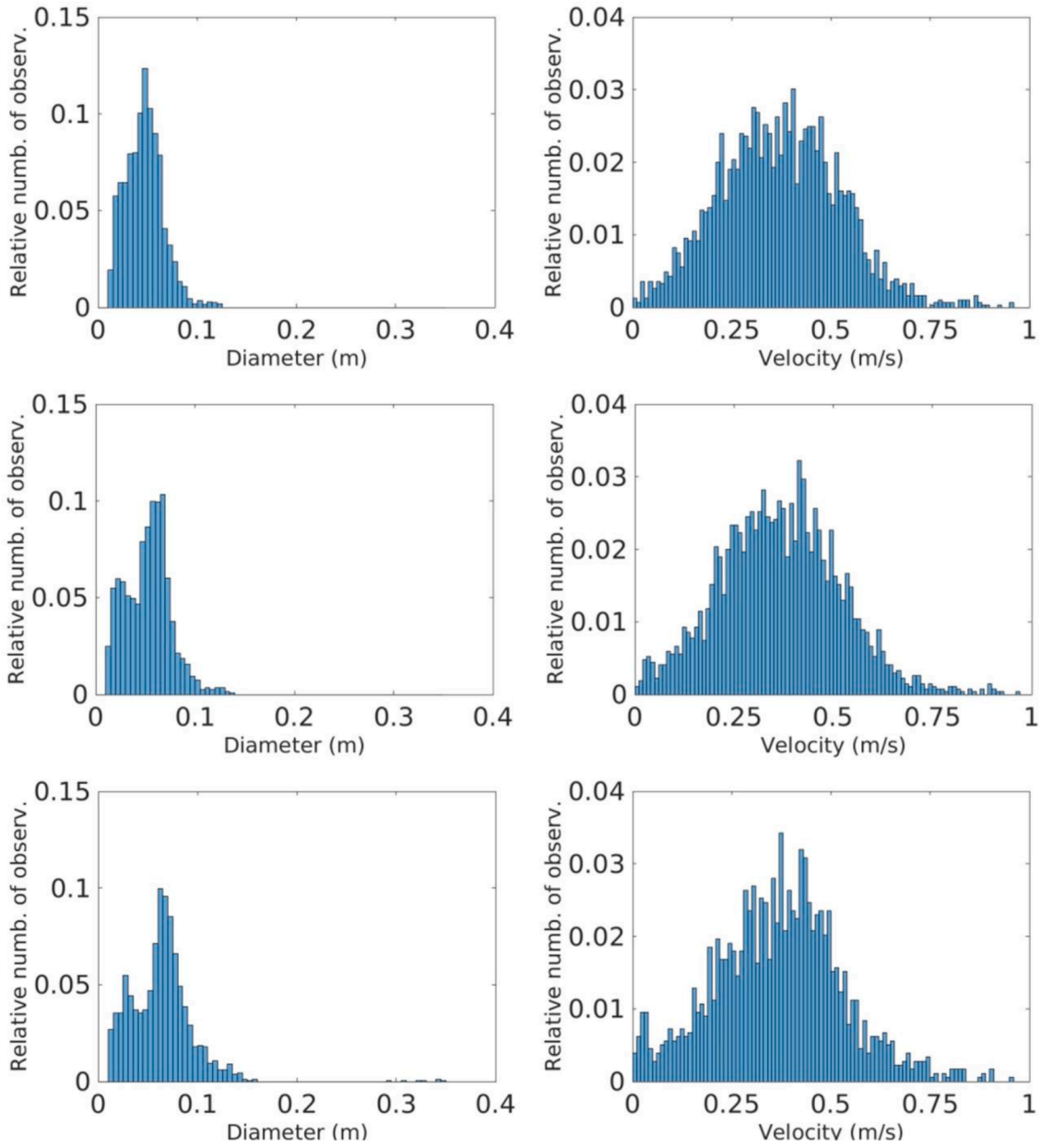

Fig. 7. SE-SMR reactor bubbles diameter and velocity distribution for the nominal flow rate=500 m^3/h of steam/methane. Top α^{th} =0.2, middle α^{th} =0.3, bottom α^{th} =0.4.

larger void zones are present throughout the bed. Bubbles diameters distribution is obviously threshold dependent, together with the total number of bubbles (Fig. 6 and 7). This is due to the fact that the transition from void to emulsion phase occurs gradually, passing from a zero particles volume fraction to the emulsion values. In the literature (Acosta-Iborra et al., 2011) different authors have used different threshold values for the volume fraction that defines bubbles contour. The higher is the particle volume fraction threshold, the larger are the bubbles detected. In the bubbling regime the adoption of a lower volume fraction threshold implies that some bubbles are miscounted. On the contrary, in the incipient slugging regime, since the domain is occupied by wider pseudo void regions, the choice of a lower volume fraction threshold causes the fragmentation of such zones and an increase in the bubbles number. It is also clear form Fig. 7 how the velocity distribution is not affected by the threshold used. In the bubbling regime for the nominal flow rate, a larger number of small bubbles are identified in the deeper layers of the fluidized bed and the bubbles number reduces upward because of coalescence, as their sizes increase.

As a general trend, bubbles dimensions and velocities increase rapidly at the beginning and slowly later during the rising (Fig. 8), except toward the bed free surface (Height>0.4 m), where the observed decrease is caused by the fact that they are cut by the free surface. The same applies for bubbles velocities and for all the thresholds used (the plots not reported for brevity). This behavior is qualitatively consistent with what is known in the literature and described by empirical formulas (Darton et al., 1977; Davidson and Harrison, 1963). A quantitative comparison is however not possible because of chemical reactions, with the consequent changes in composition, temperatures and physical properties, in the present case. In Fig. 9 bed expansion is represented. Since the height of the initial packed bed is about 0.42 m, the maximum bed expansion is about 0.15 m (double arrow in Fig. 9) at the maximum gas flow rate simulated.

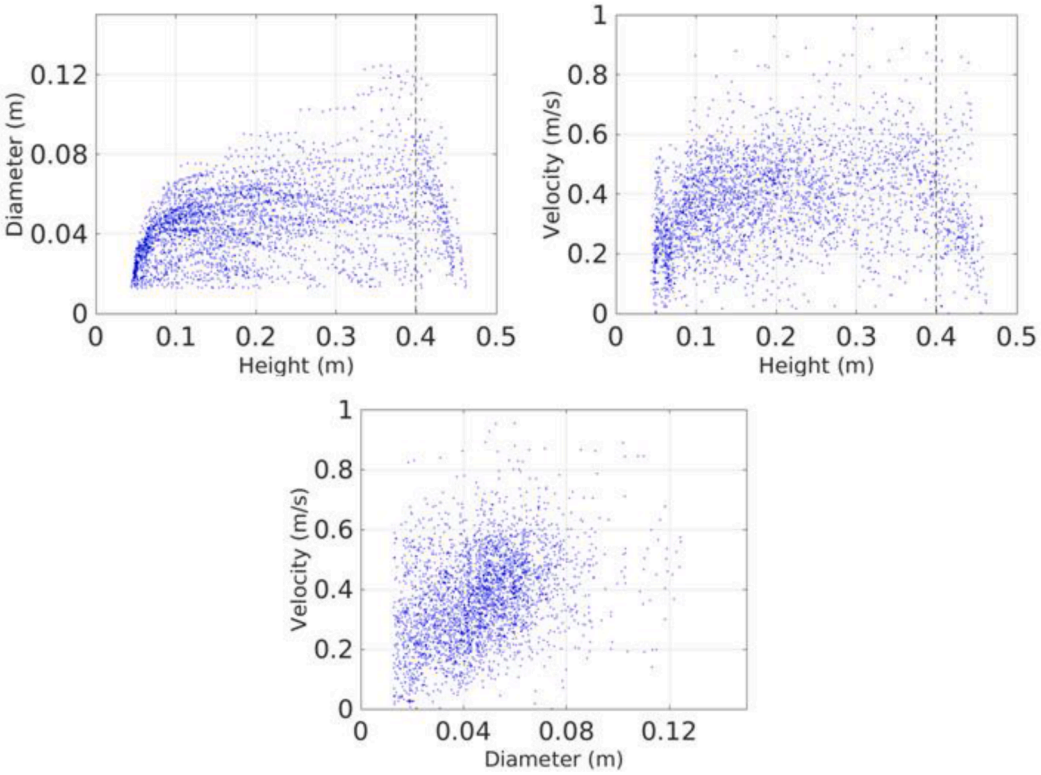

Fig. 8. SE-SMR reactor bubbles diameter vs height, velocity vs height and velocity vs diameter scatter plots for the nominal flow rate=500 m^3/h of steam/methane and α^{th}=0.2.

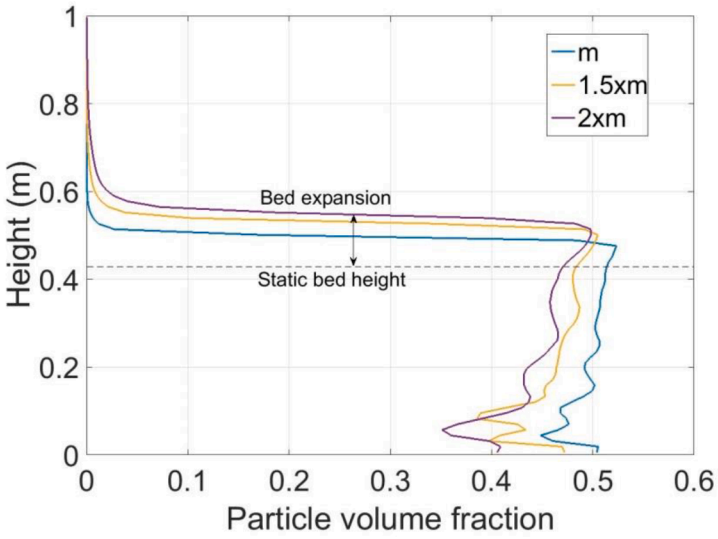

Fig. 9. SE-SMR reactor fluidized bed expansion height. Blue: nominal flow rate=500 m^3/h of steam/methane. Yellow: 1.5xnominal flow rate. Purple: 2xnominal flow rate.

6.2. *Operating conditions sensitivity analysis*

The SE-SMR process has been simulated using for the reactor initial hold-up different sorbent compositions, i.e. from fully calcined dolomite particles to 75% converted particles. The boundary conditions are reported in Fig. 2 and Table 2. The catalyst diameter has been adjusted for each conversion level, to eliminate the influence of catalyst segregation, since the weight of the sorbent particle changes with conversion. Both the XF and NK have been adopted as chemical reactions mechanisms. For the subsequent simulations a mesh of 100000 cubic cells for the entire reactor height has been adopted, that ensures grid independency in relation to the product gas composition. The simulations time used for the following sensitivity analysis (1 min) is that needed to reach a "quasi-steady" gas composition at the reactor exit. In this time interval conversion doesn't change appreciably and the mass introduced with the fresh sorbent material (calcined dolomite) is negligible, compared to the initial sorbent mass in the bed. In this way the results obtained are relative to the reactor initial hold-up sorbent composition and conversion. For a much longer simulation time the mean sorbent conversion and accordingly the product gas composition clearly change, but very

slowly.

In Fig. 10 hydrogen and carbon dioxide concentration profiles are reported as a function of sorbent composition in the reactor initial hold-up. The dry hydrogen content in the product gas attains values higher than 96% for the XF mechanism and higher than 94% for the NK mechanism, when a fresh sorbent (fully calcined dolomite) is used. It begins to decrease as the sorbent conversion increases and less CO_2 is captured, but remains still higher than 80% (both mechanisms), even when the sorbent has almost exhausted its capture capacity. The two mechanisms predict similar concentration values, with the XF mechanism that tends to predict slightly higher hydrogen contents compared to the NK mechanism. At the same time, a more and more higher content of unconverted methane is found in the product gas with an increasing sorbent conversion. The differences between the two mechanisms are more pronounced in this regard. For the XF mechanism methane conversion is in the range 98.5-94.7%, while for the NK mechanism is in the range 96.1-88.8%.

One single simulation has been executed at this point for a sufficient long simulation time using a coarser mesh, in order to obtain the steady state sorbent mean composition for the nominal operating conditions, resulting from a continuous feed of fully calcined particles. The simulation time needed to reach a steady mean conversion is of the order of 1 h and the XF mechanism has been used. The corresponding sorbent mean conversion level is about 60% and it has been used for the sorbent composition of the reactor initial hold-up in the following sensitivity analysis cases (Fig. 11). The effects of the fluidizing gas mass flow rate and the sorbent to catalyst mass ratio have been evaluated on the finer mesh (Fig. 11), using the XF mechanism. As the catalyst mass is reduced, the product gas hydrogen content decreases, because the lower amount of catalyst reduces steam methane reforming reactions rates and CH_4 conversion. When the fluidizing gas flow is increased, a reduction of H_2 content is obtained as well (Fig. 11). As we have seen above, since bubbles sizes grow with the increase of gas superficial velocity, more and more quantity of the inlet reacting gas mixture, enclosed in the bubbles, is partially inhibited from particles contact and from catalytic and CO_2 capture reactions. For this reason is advisable to avoid large bubbles formation, that penalizes process efficiency. Furthermore the gas/particles contact time is lower, due to the general higher velocities and a larger amount of CH_4, for a fixed catalyst load, has to be converted.

A comparison between the proposed full-loop and the current systems can be easily done, on the basis of the results reported in Fig. 10. For the proposed system the steady sorbent conversion is about 60% and the corresponding steady hydrogen concentration is about 83-86%. For the current batch system no steady conditions can be clearly reached and, as the sorbent conversion increases during the process, the corresponding hydrogen concentration decreases and can be read again from Fig. 10. It should be noted that in order for the two systems to operate at the same operating temperature, the batch system must be fed with a steam/methane flow at a higher temperature than the one adopted in the proposed closed loop, since in the latter case there is an extra thermal input, due to the hot solid material coming from the calciner.

Many industrial processes use fluidized bed reactors composed of particles of different sizes and properties. A certain degree of stratification of one component with respect to the others can be accepted. The level of mixing of the solid components of a binary mixture is the results of bubbles action on particles with different sizes and densities, which causes a substantial difference in the drag per unit weight. In the present case sorbent and catalyst particles segregation represents a source of inefficiency for the steam methane reforming and CO_2 capture processes, since reactions are restricted to a limited portion of the entire bed and for a limited contact time. To confirm that hypothesis, additional simulations have been conducted comparing different cases. The catalyst diameter has been adjusted until segregation (at the top of the bed) in one case (250 μm) and good mixing for the second one (380 μm) occurs (Fig. 12). In Table 3 the mixing index of those cases is reported. The mixing index (Lacey, 1943) is calculated by the variance of the catalyst particles volume fraction distribution throughout the bed:

$$M = 1 - \frac{var}{var_0} \tag{33}$$

where var_0 is the variance of the catalyst volume fraction distribution of a totally unmixed system (the catalyst is segregated completely on the top of the particle bed) and is equal to 0.0355 for this case. A value of M close to 1 indicates a perfectly mixed system.

As it is clear from Fig. 11, there is a remarkable difference in the obtained gas composition. When no segregation occurs, the product gas is richer in hydrogen by over 8 percentage points. In fact, if segregation occurs, the steam methane reforming reactions are concentrated just in the upper portion of the bed and in addition the CO_2 produced is captured only by the upper sorbent layers in the bed, while the deeper layers are ineffective. In this regard a catalyst segregation in the bottom part of the bed would be less disadvantageous, since at least the sorption process would interest the entire material. For catalyst diameters higher than 380 μm the mixing index starts to reduce. Therefore, the correct

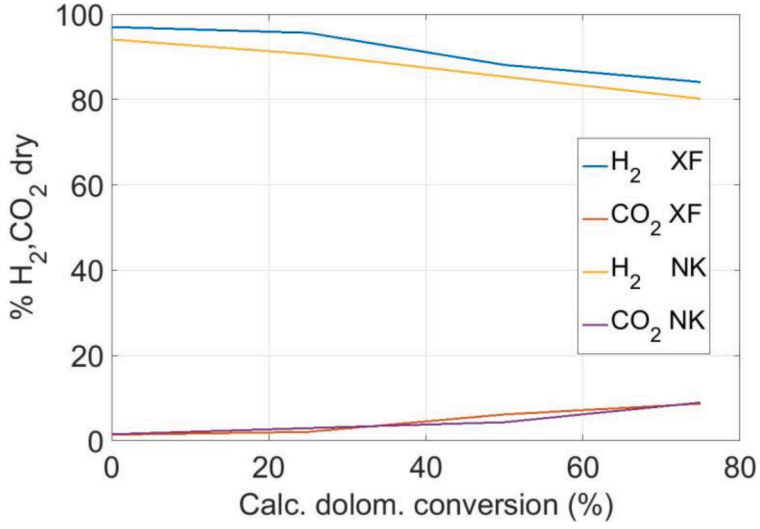

Fig. 10. SE-SMR reactor hydrogen and carbon dioxide concentration in the product gas, for the nominal operating conditions, as a function of sorbent composition (i.e. calcined dolomite conversion) in the reactor initial hold-up: from fully calcined dolomite particles to 75% converted particles. XF: Xu and Froment mechanism. NK: Numaguchi and Kikuchi mechanism.

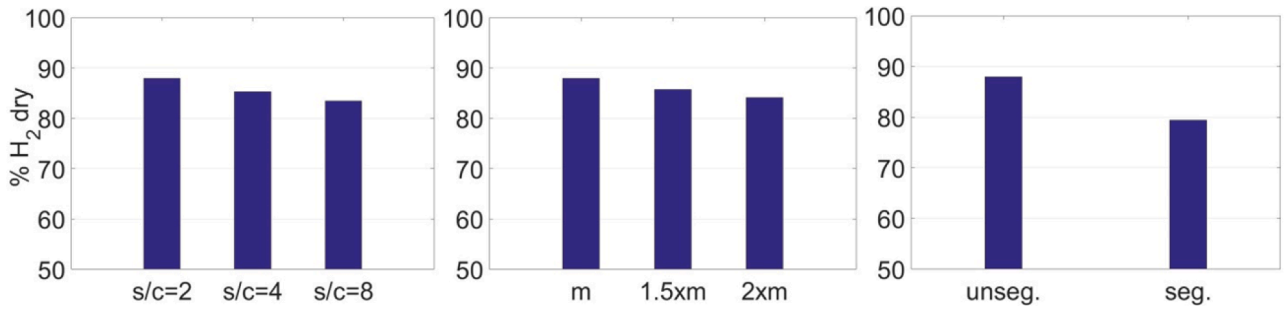

Fig. 11. SE-SMR reactor hydrogen concentration in the product gas sensitivity analysis. s/c: sorbent to catalyst mass ratio. m: steam/methane flow 500 m^3/h. unseg. and seg.: catalyst particles unsegregated and segregated cases.

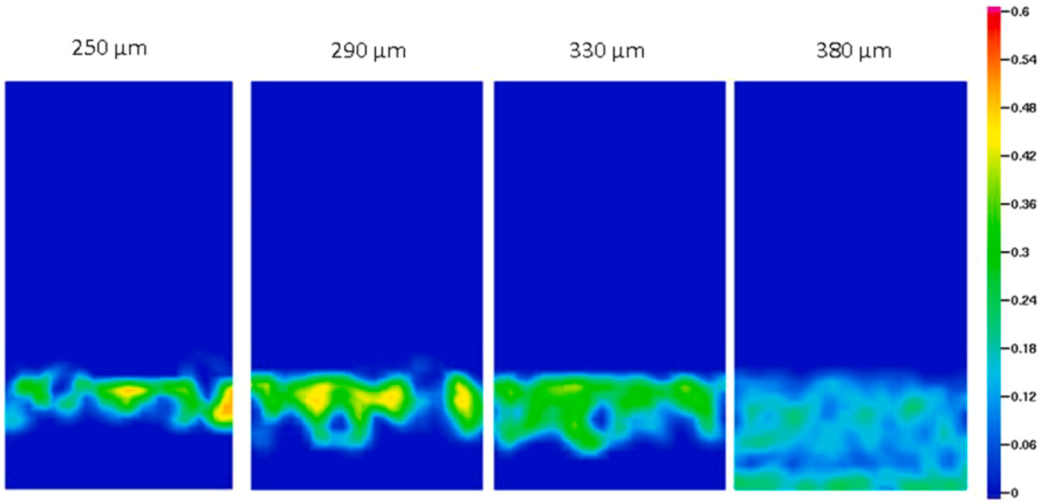

Fig. 12. Catalyst segregation. SE-SMR reactor catalyst volume fraction at different catalyst particles diameters.

Table 3
Sorbent and catalyst mixing index in the carbonator reactor.

Catalyst Diameter (µm)	M
250	0
270	0.10
290	0.17
310	0.21
330	0.34
340	0.55
360	0.78
380	0.84

choice of particles sizes represents a crucial point for the efficient operation of the carbonator reactor. However, in a real case the bed material inventory is more probably composed by particles characterized by a certain distribution of conversion levels, sizes and densities, that in part attenuate the risk of segregation, since is less probable for the catalyst particles to be "heavier" or "lighter" than the sorbent particles.

7. Sizing and simulation of a calciner reactor for sorbent regeneration

The choice of the drag model is crucial for the correct prediction of the heterogeneous structures in a riser. The classical homogenous drag models revealed some limitations and inaccuracies, especially for coarse meshes. The EMMS drag model belongs to the heterogeneous drag models and it based on the hypothesis that the flow can decomposed in different scales. At micro-scale level, the model accounts for particle-fluid interaction in the dense (clusters) and diluted phase, while at meso-scale level it accounts for dilute-dense phases interactions. For those reasons, for the modelling and simulation of the calciner the EEMS drag model has been adopted. After some simulations and tuning of the main parameters involved in the process, the obtained calciner reactor to be integrated in the ECCSEL Research Infrastructure ZECOMIX is a 7 m high cylinder of diameter 0.285 m. The reactor is fluidized by a hot gas flow (85% CO_2, 13% H_2O, 2% O_2) of 1100 m^3/h at 1527°C, that will be generated by the mixing of a CO_2 stream with the exhaust gas flow produced by an oxy-burner and 238 kg/h of 60% converted calcined dolomite (corresponding to the converted 188 kg/h of calcined dolomite introduced in the carbonator) and 94 kg/h of catalyst (the same introduced in the carbonator, since it doesn't react or change weight in the loop) at 650°C (Fig. 13, Table 4) are the solid material inlet flows. The burner must be necessarily an oxy-burner in order to avoid the introduction of nitrogen with combustion air and obtain a very CO_2 concentrated product gas at the calciner exit. The system is in the fast fluidization regime and is operated at atmospheric pressure. At atmospheric pressure a temperature in the range 850-950°C is needed to achieve calcination, according to equilibrium constraints. At higher pressures, higher temperatures are necessary. Furthermore, in this way the temperature gap between carbonator and calciner is minimized and particles lifetime is increased.

The results in Fig. 14 clearly show how the bottom-dense, upper-dilute and core-annulus heterogeneous structures are captured by the EMMS drag model, with the classical void fraction profiles in the axial

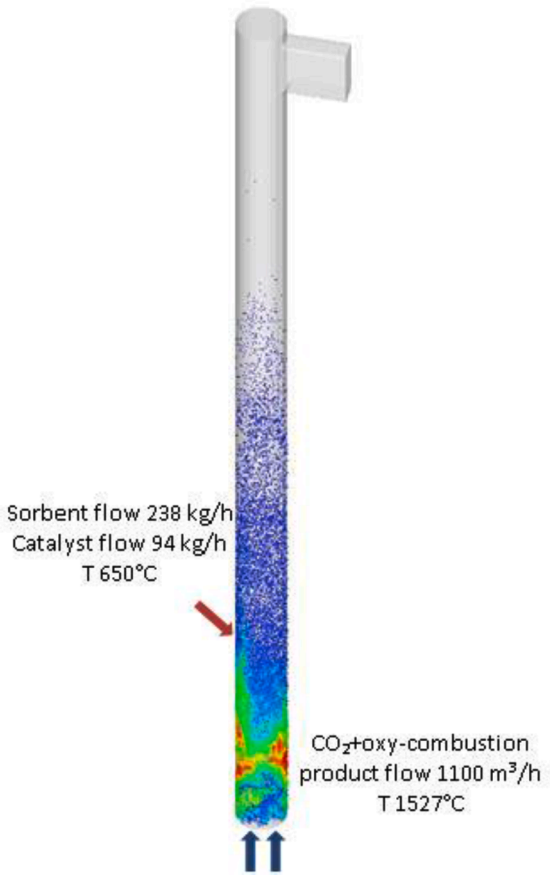

Fig. 13. Calciner operating conditions.

Table 4
Calciner operating condition.

Fluidizing gas flow	1100 m^3/h
Fluidizing gas temperature	1527°C
Exhaust sorbent mass flow	238 kg/h
Catalyst mass flow	94 kg/h
Exhaust sorbent and catalyst temp.	650°C
Operating pressure	1 atm

direction and solid volume fraction in the radial direction. This is crucial for the correct prediction of the residence time and the sorbent regeneration level. It is known that with homogenous drag models the residence time is not correctly predicted and this leads to an incorrect sizing of the riser. Particles residence time, conversion and temperature distribution, taken at the reactor exit, are reported in Fig. 15. The mean residence time is about 82 s, which allows the particles to rise their temperature up to a mean value of 923°C, which is high enough to achieve a good regeneration. In fact, almost 80% of the exhausted sorbent particles experiences complete regeneration.

8. Conclusions

This works discusses the CPFD simulations results of a SE-SMR process for H_2 production. The case study is the bubbling fluidized bed batch reactor of the ECCSEL research infrastructure ZECOMIX, when it is operated in continuous mode, with the addition of a fast riser used to regenerate the sorbent.

In this paper we have formulated and developed a straightforward method for bubbles detection to post-process simulations results. The irregular surface and the shape complexity are reconstructed using the 3D alpha-shape algorithm. The bubbles size distribution and the total number of bubbles has demonstrated to be dependent on the assumed particles volume fraction threshold, since the transition from the void (i.e. bubble) to the emulsion phase occurs gradually, through the wake phase, where the void fraction is between 0 and 1. A parametric analysis has been conducted by increasing the superficial velocity from its nominal value up to its double value: as the superficial velocity increases the bubbles grow in size and the transition from bubbling to slugging fluidization regime appears. In the bubbling regime the high number of small bubbles in the deeper layers of the bed reduces as they rise and grow because of gas entrainment and coalescence. Moreover, after a rapid acceleration and growth at the beginning of the rise, bubbles velocities and equivalent diameters continue to increases but at a slower rate.

For what concerns model validation, the agreement between the experimental data, relating to a laboratory system, and the numerical simulations has been found to be quite good. The model has been able to predict for example the slight reduction in hydrogen concentration as the operating temperature decreases. The adoption of the CPFD model has made it possible to carry out detailed 3D simulations for a very long simulation time, allowing to calculate sorbent particles average conversion at the steady state regime. Moreover, the EMMS drag model has proved capable of capturing the heterogeneous structures in the riser, where the homogeneous drag models fails.

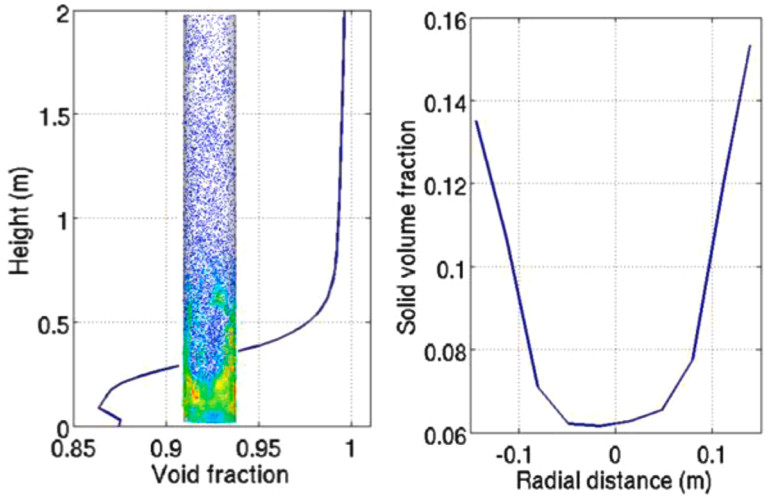

Fig. 14. Calciner axial void fraction (left) and radial (at Height=0.6 m) particles volume fraction (right).

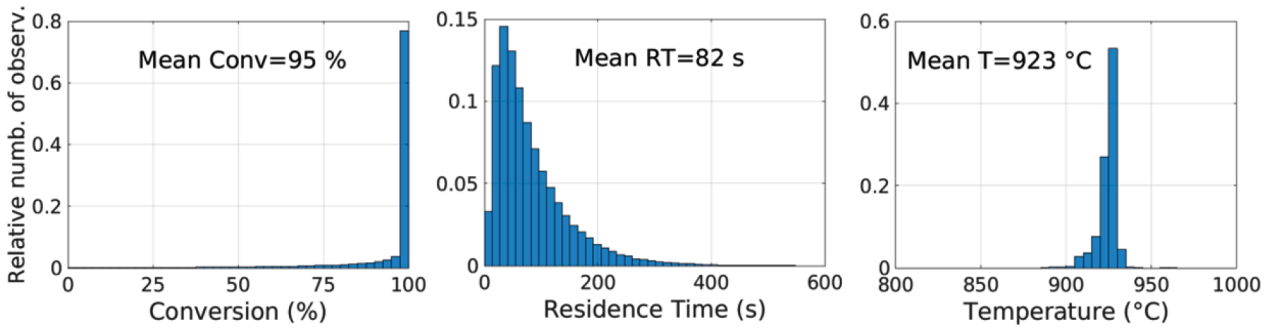

Fig. 15. Calciner exhaust sorbent particles conversion, residence time and temperature at the calciner exit.

The XF and the NK chemical kinetic mechanisms have been compared for different sorbent compositions and some differences have been noticed regarding CO_2 and H_2 content in the output gas. In case of fresh sorbent, the dry hydrogen content in the product gas has been higher than 96% for the XF mechanism and higher than 94% for the NK mechanism. With both mechanisms, concentrations higher than 80% have been obtained when the sorbent is almost exhausted. In general, with the XF mechanism higher hydrogen contents and higher methane conversions have been calculated. Both mechanisms have been extensively used for the modelling of SMR process but never compared in such kind of simulations.

A sensitivity analysis has been conducted to evaluate the influence of sorbent to catalyst ratio, steam/methane flow and catalyst segregation on the product gas H_2 concentration. By increasing the sorbent/catalyst ratio or the steam/methane flow, a maximum reduction of five percentage points of H_2 concentration has been obtained, in both cases. A decrease of eight percentage points of H_2 concentration has been instead obtained when catalyst is completely segregated.

With the aim to make the ZECOMIX process continuous through the creation of a closed loop, a calciner for the regeneration of the solid sorbent material has been dimensioned. The calciner has been conceived as a fast riser, able to regenerate the spent solid within a cylinder having an inner diameter of 0.285 m and a height of 7 m. A mean residence time of 82 s has demonstrated to be enough to achieve an almost complete calcination of the sorbent particles.

For what regards the proposed closed loop system performance, hydrogen concentration in the product gas and methane conversion are very good using a fresh sorbent. This suggests increasing the sorbent solid flow between the two reactors, reducing its residence time in the SE-SMR reactor in order to have on average less converted material and with a greater capture capacity. If this is clearly possible in a CFB such as the one studied here, it is not practicable in batch systems, that represent almost all of those described in the literature. In the end, the advantage given by the proposed continuous system is above all of an operational nature. In fact, in order to maintain a good capture capacity in the current batch reactor, it is necessary to frequently interrupt the process and regenerate the sorbent, by the switching of the fluidization gas composition and temperature, with an inevitable lower productivity and a more complicated management.

Funding

The research leading to these results was funded by the European Union's Seventh Framework Program ASCENT grant agreement no 608512 and by the Italian Ministry of Economic Development, under the project SFERO (Systems for Flexible Energy via Reuse of carbOn) grant number CUP I34I19005780001 within the Italian research programme 2019-2021: "Ricerca di Sistema".

CRediT authorship contribution statement

Antonio Di Nardo: Conceptualization, Methodology, Software, Validation, Formal analysis, Writing – original draft, Writing – review & editing, Visualization, Supervision. **Giorgio Calchetti:** Conceptualization, Software, Validation, Writing – review & editing, Visualization. **Andrea Di Carlo:** Conceptualization, Validation, Writing – review & editing. **Stefano Stendardo:** Conceptualization, Writing – review & editing, Project administration, Funding acquisition.

Declaration of Competing Interest

The authors declare that they have no known competing financial interests or personal relationships that could have appeared to influence the work reported in this paper. The authors declare the following financial interests/personal relationships which may be considered as potential competing interests.

Acknowledgment

The computing resources and the related technical support used for this work have been provided by CRESCO/ENEAGRID High Performance Computing infrastructure and its staff. CRESCO/ENEAGRID High Performance Computing infrastructure is funded by ENEA, the Italian National Agency for New Technologies, Energy and Sustainable Economic Development and by Italian and European research programs, see http://www.cresco.enea.it/english for information.

References

Abbas, S.Z., Dupont, V., Mahmud, T., 2019. Modelling of H_2 production via sorption enhanced steam methane reforming at reduced pressures for small scale applications. Int. J. Hydrog. Energy 44, 1505–1513. https://doi.org/10.1016/j.ijhydene.2018.11.169.

Acosta-Iborra, A., Sobrino, C., Hernandez-Jimenez, F., de Vega, M., 2011. Experimental and computational study on the bubble behavior in a 3-D fluidized bed. Chem. Eng. Sci. 66, 3499–3512. https://doi.org/10.1016/j.ces.2011.04.009.

Aloisi, I., Di Giuliano, A., Di Carlo, A., Foscolo, P.U., Courson, C., Gallucci, K., 2017. Sorption enhanced catalytic steam methane reforming: experimental data and simulations describing the behaviour of bi-functional particles. Chem. Eng. J. 314, 570–582. https://doi.org/10.1016/j.cej.2016.12.014.

Baker, M.C., Kong, B., Capecelatro, J., Desjardins, O., Fox, R.O., 2020. Direct comparison of Eulerian-Eulerian and Eulerian-Lagrangian simulations for particle-laden vertical channel flow. AIChE J 66, e16230. https://doi.org/10.1002/aic.16230.

Chao, Z., Zhang, Y., Wang, Y., Jakobsen, J.P., Jakobsen, H.A., 2017. Modelling of binary fluidized bed reactors for the sorption-enhanced steam methane reforming process. Can. J. Chem. Eng. 95, 157–169. https://doi.org/10.1002/cjce.22602.

Chen, C., Werther, J., Heinrich, S., Qi, H.Y., Hartge, E.U., 2013a. CPFD simulation of circulating fluidized bed risers. Powder Technol. 235, 238–247. https://doi.org/10.1016/j.powtec.2012.10.014.

Chen, Y., Zhao, Y., Zheng, C., Zhang, J., 2013b. Numerical study of hydrogen production via sorption-enhanced steam methane reforming in a fluidized bed reactor at relatively low temperature. Chem. Eng. Sci. 92, 67–80. https://doi.org/10.1016/j.ces.2013.01.024.

Clark, S., Snider, D.M., Spenik, J., 2013. CO_2 Adsorption loop experiment with Eulerian–Lagrangian simulation. Powder Technol 242, 100–107. https://doi.org/10.1016/j.powtec.2013.01.011.

de Smet, C.R.H., de Croon, M.H.J.M., Berger, R.J., Marin, G.B., Schouten, J.C., 2001. Design of adiabatic fixed-bed reactors for the partial oxidation of methane to synthesis gas. Application to production of methanol and hydrogen-for-fuel-cells. Chem. Eng. Sci. 56, 4849–4861. https://doi.org/10.1016/S0009-2509(01)00130-0.

Deen, N.G., Van Sint Annaland, M., Van der Hoef, M.A., Kuipers, J.A.M., 2007. Review of discrete particle modeling of fluidized beds. Chem. Eng. Sci. 62, 28–44. https://doi.org/10.1016/j.ces.2006.08.014.

Darton, R.C., LaNauze, R.D., Davidson, J.F., Harrison, D., 1977. Bubble growth due to coalescence in fluidised beds. Trans. Inst. Chem. Eng. 55, 274.

Davidson, J.F., Harrison, D., 1963. Fluidized Particles. Cambridge University Press, London.

Di Carlo, A., Bocci, E., Zuccari, F., Dell'Era, A., 2010. Numerical investigation of sorption enhanced steam methane reforming process using computational fluid dynamics Eulerian-Eulerian code. Ind. Eng. Chem. Res. 49 (4), 1561–1576. https://doi.org/10.1021/ie900748t.

Di Carlo, A., Aloisi, I., Jand, N., Stendardo, S., Foscolo, P.U., 2017. Sorption enhanced steam methane reforming on catalyst-sorbent bifunctional particles: A CFD fluidized bed reactor model. Chem. Eng. Sci. 173, 428–442. https://doi.org/10.1016/j.ces.2017.08.014.

Diglio, G., Hanab, D.P., Bareschino, P., Pepe, F., Montagnaro, F., Manovic, V., 2018. Modelling of sorption-enhanced steam methane reforming in a fixed bed reactor network integrated with fuel cell. Appl. Energy 210, 1–15. https://doi.org/10.1016/j.apenergy.2017.10.101.

Edelsbrunner, H., Mücke, E.P., 1994. Three-Dimensional Alpha Shapes. ACM Trans. Graphics 13, 43–72. https://doi.org/10.1145/174462.156635.

Faheem, H.H., Tanveer, H.U., Syed, Z., Abbas, S.Z., Maqbool, F., 2021. Comparative study of conventional steam-methane-reforming (SMR) and auto-thermal-reforming (ATR) with their hybrid sorption enhanced (SE-SMR & SE-ATR) and environmentally benign process models for the hydrogen production. Fuel 297, 120769. https://doi.org/10.1016/j.fuel.2021.120769.

Fan, L.S., Zhu, C., 1998. Principles of Gas-Solid Flows. Cambridge University Press, New York.

Fang, F., Li, Z.S., Cai, N.S., 2009. Experiment and modeling of CO_2 capture from flue gases at high temperature in a fluidized bed reactor with Ca-based sorbents. Energy Fuels 23, 207–216. https://doi.org/10.1021/ef800474n.

Feng, M., Li, F., Wang, W., Li, J., 2018. Parametric study for MP-PIC simulation of bubbling fluidized beds with Geldart A particles. Powder Technol 328, 215–226. https://doi.org/10.1016/j.powtec.2018.01.024.

Gidaspow, D., 1994. Multiphase Flow and Fluidization: Continuum and Kinetic Theory Descriptions. American Press, Boston. https://doi.org/10.1002/aic.690420438.

Gidaspow, D., Jung, J., Singh, R.K., 2004. Hydrodynamics of fluidization using kinetic theory: an emerging paradigm: 2002 Flour-Daniel lecture. Powder Technol 148, 123–141. https://doi.org/10.1016/j.powtec.2004.09.025.

Huang, W.J., Yu, C.T., Sheu, W.J., Chen, Y.C., 2021. The effect of non-uniform temperature on the sorption-enhanced steam methane reforming in a tubular fixed-bed reactor. Int. J. Hydrog. Energy 46, 16522–16533. https://doi.org/10.1016/j.ijhydene.2020.07.182.

IEA, 2019. The Future of Hydrogen. Seizing today's opportunities. Report prepared by the IEA for the G20, Japan. https://www.iea.org/topics/hydrogen/.

Julián, I., González, D., Herguido, J., Menéndez, M., 2016. Use of α-shapes for the measurement of 3D bubbles in fluidized beds from two-fluid model simulations. Powder Technol 288, 409–421. https://doi.org/10.1016/j.powtec.2015.11.035.

Karimipour, S., Pugsley, T., 2012. Application of the particle in cell approach for the simulation of bubbling fluidized beds of Geldart A particles. Powder Technol 220, 63–69. https://doi.org/10.1016/j.powtec.2011.09.026.

Lacey, P.M.C., 1943. The mixing of solid particles. Trans. Inst. Chem. Eng. 21, 53–59.

Li, F., Song, F., Benyahia, S., Wang, W., Li, J., 2012. MP-PIC simulation of CFB riser with EMMS-based drag model. Chem. Eng. Sci. 82, 104–113. https://doi.org/10.1016/j.ces.2012.07.020.

Li, J.H., Kwauk, M., 1994. Particle-Fluid Two-Phase Flow: the Energy-Minimization Multi-Scale method. Metallurgical Industry Press, Beijing.

Liang, Y., Zhang, Y., Li, T., Lu, C., 2014. A critical validation study on CPFD model in simulating gas–solid bubbling fluidized beds. Powder Technol 263, 121–134. https://doi.org/10.1016/j.powtec.2014.05.003.

Lindborg, H., Jakobsen, H.A., 2009. Sorption enhanced steam methane reforming process performance and bubbling fluidized bed reactor design analysis by use of a two-fluid model. Ind. Eng. Chem. Res. 48, 1332–1342. https://doi.org/10.1021/ie800522p.

Liu, H., Cattolica, R.J., Seiser, R., Liao, C., 2015. Three-dimensional full-loop simulation of a dual fluidized-bed biomass Gasifier. Appl. Energy 160, 489–501. https://doi.org/10.1016/j.apenergy.2015.09.065.

Martínez, I., Grasa, G., Murillo, R., Arias, B., Abanades, J.C., 2012. Kinetics of calcination of partially carbonated particles in a Ca-looping system for CO_2 capture. Energy Fuels 26, 1432–1440. https://doi.org/10.1021/ef201525k.

Numaguchi, T., Kikuchi, K., 1988. Intrinsic kinetics and design simulation in a complex reaction network: steam-methane reforming. Chem. Eng. Sci. 43, 2295–2301. https://doi.org/10.1016/0009-2509(88)87118-5.

O'Rourke, P.J., Zhao, P., Snider, D., 2009. A model for collisional exchange in gas/liquid/solid fluidized beds. Chem. Eng. Sci. 64, 1784–1797. https://doi.org/10.1016/j.ces.2008.12.014.

Ping, H., Wu, S., 2019. The coupling performance during reactive sorption enhanced reforming (ReSER) process: simulation and experimental studies. Int. J. Hydrog. Energy 44, 26943–26954. https://doi.org/10.1016/j.ijhydene.2019.08.152.

Piomelli, U., 1999. Large-eddy simulation: achievements and challenges. Progr. Aerospace Sci. 35 (4), 335–362. https://doi.org/10.1016/S0376-0421(98)00014-1.

Shahid, M.M., Abbas, S.Z., Maqbool, F., Ramirez-Solis, S., Dupont, V., Mahmud, T., 2021. Modeling of sorption enhanced steam methane reforming in an adiabatic packed bed reactor using various CO_2 sorbents. J. Environ. Chem. Eng. 9, 105863 https://doi.org/10.1016/j.jece.2021.105863.

Shi, Z., Wang, W., Li, J., 2011. A bubble-based EMMS model for gas–solid bubbling fluidization. Chem. Eng. Sci. 66, 5541–5555. https://doi.org/10.1016/j.ces.2011.07.020.

Smagorinsky, J., 1963. General circulation experiments with the primitive equations. Monthly Weather Rev. 91 (3), 99–164.

Snider, D., Banerjee, S., 2010. Heterogeneous gas chemistry in the CPFD Eulerian-Lagrangian numerical scheme (ozone decomposition). Powder Technol. 199, 100–106. https://doi.org/10.1016/j.powtec.2009.04.023.

Snider, D.M., 2001. An incompressible three-dimensional multiphase particle-in-cell model for dense particle flows. J. Comput. Phys. 170, 523–549. https://doi.org/10.1006/jcph.2001.6747.

Snider, D.M., Clark, S.M., O'Rourke, P.J., 2011. Eulerian-Lagrangian method for three dimensional thermal reacting flow with application to coal gasifiers. Chem. Eng. Sci. 66, 1285–1295. https://doi.org/10.1016/j.ces.2010.12.042.

Stanmore, B.R., Gilot, P., 2005. Review-calcination and carbonation of limestone during thermal cycling for CO_2 sequestration. Fuel Process. Technol. 86, 1707–1743. https://doi.org/10.1016/j.fuproc.2005.01.023.

Stendardo, S., Foscolo, P.U., 2009. Carbon dioxide capture with dolomite: a model for gas–solid reaction within the grains of a particulate sorbent. Chem. Eng. Sci. 64, 2343–2352. https://doi.org/10.1016/j.ces.2009.02.009, 2009.

Thapa, R.K., Frohner, A., Tondl, G., Pfeifer, C., Halvorsen, B.M., 2016. Circulating fluidized bed combustion reactor: computational particle fluid dynamic model validation and gas feed position optimization. Comput. Chem. Eng. 92, 180–188. https://doi.org/10.1016/j.compchemeng.2016.05.008.

Tu, Q., Wang, H., 2018. CPFD study of a full-loop three-dimensional pilot-scale circulating fluidized bed based on EMMS drag model. Powder Technol. 323, 534–547. https://doi.org/10.1016/j.powtec.2017.09.045.

Wang, Y., Chao, Z., Jakobsen, H.A., 2011. Numerical study of hydrogen production by the sorption-enhanced steam methane reforming process with online CO_2 capture as operated in fluidized bed reactors. Clean Techn. Environ. Policy 13, 559–565. https://doi.org/10.1007/s10098-011-0368-y.

Wang, J., Wang, Y., Jakobsen, H.A., 2014. The modeling of circulating fluidized bed reactors for SE-SMR process and sorbent regeneration. Chem. Eng. Sci. 108, 57–65. https://doi.org/10.1016/j.ces.2013.12.012.

Xu, J., Froment, G.F., 1989. Methane steam reforming, methanation and water gas shift: I. Intrinsic kinetics. AIChE J 35, 88–96. https://doi.org/10.1002/aic.690350109.

Yang, W.C., 2003. Handbook of Fluidization and Fluid-Particle Systems. Marcell Dekker, Inc., New York.

Zhang, Y., Lu, X.B., Zhang, X.H., 2021. An optimized Eulerian-Lagrangian method for two-phase flow with coarse particles: Implementation in open-source field operation and manipulation, verification, and validation. Phys. Fluids 33, 113307. https://doi.org/10.1063/5.0067553.

Zhu, H.P., Zhou, Z.Y., Yang, R.Y., Yu, A.B., 2007. Discrete particle simulation of particulate systems: theoretical developments. Chem. Eng. Sci. 62, 3378–3396. https://doi.org/10.1016/j.ces.2006.12.089.